

Maximizing the electromagnetic chirality of thin dielectric tubes

Tilo Arens, Roland Griesmaier, Marvin Knöller

CRC Preprint 2021/3, January 2021

KARLSRUHE INSTITUTE OF TECHNOLOGY

CRC 1173



Wave
phenomena

Participating universities



Universität Stuttgart

EBERHARD KARLS
UNIVERSITÄT
TÜBINGEN



Funded by

DFG

Maximizing the electromagnetic chirality of thin dielectric tubes

Tilo Arens, Roland Griesmaier and Marvin Knöller*

January 21, 2021

Abstract

Any time-harmonic electromagnetic wave can be uniquely decomposed into a left and a right circularly polarized component. The concept of electromagnetic chirality (em-chirality) describes differences in the interaction of these two components with a scattering object or medium. Such differences can be quantified by means of em-chirality measures. These measures attain their minimal value zero for em-achiral objects or media that interact essentially in the same way with left and right circularly polarized waves. Scattering objects or media with positive em-chirality measure interact qualitatively different with left and right circularly polarized waves, and maximally em-chiral scattering objects or media would not interact with fields of either positive or negative helicity at all. This paper examines a shape optimization problem, where the goal is to determine thin tubular structures consisting of dielectric isotropic materials that exhibit large measures of em-chirality at a given frequency. We develop a gradient based optimization scheme that uses an asymptotic representation formula for scattered waves due to thin tubular scattering objects. Numerical examples suggest that thin helical structures are at least locally optimal among this class of scattering objects.

Mathematics subject classifications (MSC2010): 78M50, (49Q10, 78A45)

Keywords: electromagnetic scattering, chirality, shape optimization, maximally chiral objects

Short title: Maximizing the electromagnetic chirality of thin tubes

1 Introduction

This work is concerned with scattering of time-harmonic electromagnetic waves by a compactly supported isotropic dielectric object in three-dimensional free space. Using Maxwell's equations to model electromagnetic wave propagation, we can uniquely decompose any incident field as well as the corresponding scattered field away from the scatterer into left and right circularly polarized components. The concept of electromagnetic chirality (em-chirality) compares the interaction of these two components with the scattering object. Broadly speaking, a scatterer is called electromagnetically achiral (em-achiral) if it scatters incident fields of one helicity in the same way as incident fields of the opposite helicity up to a unitary transformation that swaps helicity. If this is not the case, then the scatterer is called electromagnetically chiral (em-chiral). A precise definition of em-chirality will be given below.

In the following we associate scattering objects with far field operators that map superpositions of plane wave incident fields to the far field patterns of the corresponding scattered waves. Based on this identification, scalar measures of em-chirality have recently been introduced in [16] (see also [5, 22]). These measures quantify the degree of em-chirality of a scattering object in terms of the singular values of suitable projections of the associated far field operator

*Institut für Angewandte und Numerische Mathematik, Karlsruher Institut für Technologie, Englerstr. 2, 76131 Karlsruhe, Germany (tilo.arens@kit.edu, roland.griesmaier@kit.edu, marvin.knoeller@kit.edu).

onto subspaces of left and right circularly polarized fields. They allow to compare the degree of em-chirality of different scattering objects. The scalar measures of em-chirality are zero for em-achiral scatterers, strictly positive for em-chiral scatterers, and they would attain their maximum for scatterers that do not interact with either left or right circularly polarized electromagnetic waves, i.e., scatterers that are invisible to incident fields of one helicity. It is unknown whether such maximally em-chiral scatterers exist, but even scattering objects that possess sufficiently large measures of em-chirality at optical frequencies have a number of interesting applications in photonic metamaterials (see, e.g., [14, 17, 29, 30, 32, 34]).

Throughout this work, we consider scattering objects that consist of isotropic materials, and the chiral effect merely results from the particular shapes of the scatterers. A different approach is studied in [6, 7], where electromagnetic scattering problems with scatterers that consist of chiral materials are discussed. A link between these two perspectives is provided in [2], where the Drude-Born-Fedorov constitutive relations governing the propagation of electromagnetic waves in chiral media have been derived from the linear constitutive relations for homogeneous isotropic media. This is achieved by embedding a large number of regularly spaced, randomly oriented chiral objects that are made of isotropic materials similar to the ones considered in this work.

We study a shape optimization problem, where the goal is to determine compactly supported dielectric scattering objects that possess comparatively large measures of em-chirality. Since thin helical structures have been proposed as candidates for highly em-chiral objects in the literature (see, e.g., [2, 16, 17] and the references therein), we focus on shape optimization for scatterers that are supported on thin tubular neighborhoods of smooth curves. The objective functional in this optimization problem is based on an em-chirality measure, and the evaluation of its shape derivative requires an approximation of the shape derivative of the complete far field operator. Accordingly, evaluating the shape derivatives in a traditional shape optimization scheme for electromagnetic scattering problems (see, e.g., [23, 24, 25, 31]) would require to solve a large number of Maxwell systems in each iteration step of the algorithm, which would be rather expensive. Using an asymptotic representation formula for scattered fields due to thin tubular dielectric structures that has recently been established in [12] (see also [1, 8, 19]), we develop a quasi-Newton scheme that does not require to solve a single Maxwell system during the optimization procedure. A similar approach has been used in [12] to construct an inexpensive Gauß-Newton reconstruction method for an inverse scattering problem with thin tubular scatterers. We also refer to [8, 18, 20] for related work on electric impedance tomography with thin tubular conductivity inclusions. The asymptotic representation formula from [12] gives an explicit approximation of the far field operator corresponding to thin tubular scattering objects, and we apply this formula to derive an explicit approximation of the shape derivative of this operator as well. Using vector spherical harmonics expansions of these approximations of the far field operator and of its shape derivative the objective functional in the shape optimization scheme can be evaluated efficiently. We stabilize the optimization procedure by adding proper regularization terms, and we apply the final algorithm to provide examples of optimized thin tubular em-chiral structures.

This paper is organized as follows. In the next section we introduce the mathematical setting, and we briefly review some facts concerning the notion of electromagnetic chirality. Then we consider the asymptotic representation formula for far field operators corresponding to thin tubular scattering objects in section 3. In section 4 we establish the shape derivative of the leading order term in this asymptotic expansion, and in section 5 we develop the shape optimization scheme. Numerical results are discussed in section 6, and in the appendix we provide explicit representations for the derivatives of spherical vector wave functions that are required for the numerical implementation of the optimization algorithm.

2 Electromagnetic chirality

We consider time-harmonic electromagnetic wave propagation in a homogenous background medium in \mathbb{R}^3 with constant *electric permittivity* $\varepsilon_0 > 0$ and constant *magnetic permeability* $\mu_0 > 0$. Throughout we will work with electric fields only. An *incident field* \mathbf{E}^i is an entire solution to Maxwell's equations

$$\mathbf{curl} \mathbf{curl} \mathbf{E}^i - k^2 \mathbf{E}^i = 0 \quad \text{in } \mathbb{R}^3, \quad (2.1a)$$

where $k = \omega\sqrt{\varepsilon_0\mu_0}$ denotes the *wave number* at frequency $\omega > 0$. We suppose that this incident field is scattered by a penetrable dielectric scattering object $D \subseteq \mathbb{R}^3$ that is bounded with connected complement, and that the *relative electric permittivity* and the *relative magnetic permeability* satisfy

$$\varepsilon_{r,D}(\mathbf{x}) := \begin{cases} \varepsilon_r, & \mathbf{x} \in D, \\ 1, & \mathbf{x} \in \mathbb{R}^3 \setminus \overline{D}, \end{cases} \quad \text{and} \quad \mu_{r,D}(\mathbf{x}) := \begin{cases} \mu_r, & \mathbf{x} \in D, \\ 1, & \mathbf{x} \in \mathbb{R}^3 \setminus \overline{D}, \end{cases}$$

for some $\varepsilon_r, \mu_r > 0$. Accordingly, the *total field* \mathbf{E} solves

$$\mathbf{curl}(\mu_{r,D}^{-1} \mathbf{curl} \mathbf{E}) - k^2 \varepsilon_{r,D} \mathbf{E} = 0 \quad \text{in } \mathbb{R}^3, \quad (2.1b)$$

and the *scattered field*

$$\mathbf{E}^s = \mathbf{E} - \mathbf{E}^i \quad (2.1c)$$

satisfies the *Silver-Müller radiation condition*

$$\lim_{|\mathbf{x}| \rightarrow \infty} (\mathbf{curl} \mathbf{E}^s(\mathbf{x}) \times \mathbf{x} - ik|\mathbf{x}| \mathbf{E}^s(\mathbf{x})) = 0 \quad (2.1d)$$

uniformly with respect to all directions $\hat{\mathbf{x}} := \mathbf{x}/|\mathbf{x}| \in S^2$. Every solution to (2.1) has the asymptotic behavior

$$\mathbf{E}^s(\mathbf{x}) = \frac{e^{ik|\mathbf{x}|}}{4\pi|\mathbf{x}|} (\mathbf{E}^\infty(\hat{\mathbf{x}}) + \mathcal{O}(|\mathbf{x}|^{-1})) \quad \text{as } |\mathbf{x}| \rightarrow \infty,$$

uniformly in $\hat{\mathbf{x}} = \mathbf{x}/|\mathbf{x}|$ (see, e.g., [13, thm. 6.9]). The vector function $\mathbf{E}^\infty \in L_t^2(S^2, \mathbb{C}^3)$ is called the *electric far field pattern*, where as usual $L_t^2(S^2, \mathbb{C}^3)$ denotes the vector space of square integrable tangential vector fields on the unit sphere.

An incident field is called a *plane wave* when

$$\mathbf{E}^i(\mathbf{x}; \boldsymbol{\theta}, \mathbf{A}) := \mathbf{A} e^{ik\boldsymbol{\theta} \cdot \mathbf{x}}, \quad \mathbf{x} \in \mathbb{R}^3, \quad (2.2)$$

for some *direction of propagation* $\boldsymbol{\theta} \in S^2$ and a *polarization vector* $\mathbf{A} \in \mathbb{C}^3$ that must satisfy $\mathbf{A} \cdot \boldsymbol{\theta} = 0$. We denote the corresponding electric far field pattern by $\mathbf{E}^\infty(\cdot; \boldsymbol{\theta}, \mathbf{A})$. Accordingly, a *Herglotz wave* with density $\mathbf{A} \in L_t^2(S^2, \mathbb{C}^3)$ is a superposition of plane waves

$$\mathbf{E}^i[\mathbf{A}](\mathbf{x}) := \int_{S^2} \mathbf{A}(\boldsymbol{\theta}) e^{ik\boldsymbol{\theta} \cdot \mathbf{x}} \, ds(\boldsymbol{\theta}), \quad \mathbf{x} \in \mathbb{R}^3, \quad (2.3)$$

We denote the corresponding total electric field and the scattered electric field by $\mathbf{E}[\mathbf{A}]$ and $\mathbf{E}^s[\mathbf{A}]$, respectively. Electric far field patterns $\mathbf{E}^\infty[\mathbf{A}]$ excited by Herglotz waves as incident fields are fully described by the *far field operator* $\mathcal{F}_D : L_t^2(S^2, \mathbb{C}^3) \rightarrow L_t^2(S^2, \mathbb{C}^3)$, which is defined by

$$(\mathcal{F}_D \mathbf{A})(\hat{\mathbf{x}}) := \int_{S^2} \mathbf{E}^\infty(\hat{\mathbf{x}}; \boldsymbol{\theta}, \mathbf{A}(\boldsymbol{\theta})) \, ds(\boldsymbol{\theta}), \quad \hat{\mathbf{x}} \in S^2.$$

By linearity we have that $\mathbf{E}^\infty[\mathbf{A}] = \mathcal{F}_D \mathbf{A}$.

In the following we discuss the physical notion of *chirality* for such electromagnetic scattering problems and give a short synopsis of the concepts and results that have recently been developed in [5, 16]. The traditional notion of chirality is concerned with the geometry of objects: An object is called *geometrically achiral* if a proper rigid transformation can be used to superimpose the object onto a reflected version of itself, and it is called *geometrically chiral* if this is not the case.

In the context of electromagnetic scattering, one has to take into consideration that applying a reflection also changes the incident field. A plane wave is said to be *left* or *right circularly polarized* if its polarization vector performs an anti-clockwise or clockwise circular motion (one turn per wave length) along the direction of propagation, respectively. This is equivalent to the relation

$$\mathbf{A} \pm i(\boldsymbol{\theta} \times \mathbf{A}) = 0 \quad (2.4)$$

in (2.2). Under a reflection such a plane wave is mapped to another plane wave, but this field is then of opposite helicity. We note also, that (2.4) is equivalent to the eigenvalue relation

$$k^{-1} \mathbf{curl} \mathbf{E}^i(\cdot; \boldsymbol{\theta}, \mathbf{A}) = \pm \mathbf{E}^i(\cdot; \boldsymbol{\theta}, \mathbf{A}),$$

which on the other hand can immediately be extended to more general fields. A solution to

$$\mathbf{curl} \mathbf{curl} \mathbf{U} - k^2 \mathbf{U} = 0 \quad \text{in } \Omega \subseteq \mathbb{R}^3 \quad (2.5)$$

is said to have *helicity* ± 1 , if \mathbf{U} is an eigenfunction of the operator $k^{-1} \mathbf{curl}$ for the eigenvalue ± 1 , respectively. Using the Beltrami fields

$$\mathbf{U} \pm k^{-1} \mathbf{curl} \mathbf{U} \quad (2.6)$$

it is easily checked that every solution to (2.5) can be decomposed into a sum of two fields of helicity $+1$ and -1 , respectively.

Returning to the scattering problem (2.1) with Herglotz waves as incident fields, both the incident field $\mathbf{E}^i[\mathbf{A}]$ and the far field pattern $\mathbf{E}^\infty[\mathbf{A}]$ are uniquely determined by the density $\mathbf{A} \in L_t^2(S^2, \mathbb{C}^3)$. Since Rellich's lemma implies a one-to-one correspondance between the scattered field $\mathbf{E}^s[\mathbf{A}]$ in $\mathbb{R}^3 \setminus \bar{D}$ and its far field pattern $\mathbf{E}^\infty[\mathbf{A}]$ (see, e.g., [13, thm. 6.10]), the same is true for $\mathbf{E}^s[\mathbf{A}]|_{\mathbb{R}^3 \setminus \bar{D}}$. To describe the helicities of $\mathbf{E}^i[\mathbf{A}]$ and $\mathbf{E}^s[\mathbf{A}]|_{\mathbb{R}^3 \setminus \bar{D}}$ in terms of \mathbf{A} , we generalize (2.4) and introduce the self-adjoint operator $\mathcal{C} : L_t^2(S^2, \mathbb{C}^3) \rightarrow L_t^2(S^2, \mathbb{C}^3)$ with

$$\mathcal{C}\mathbf{A}(\boldsymbol{\theta}) = i\boldsymbol{\theta} \times \mathbf{A}(\boldsymbol{\theta}), \quad \boldsymbol{\theta} \in S^2.$$

We note that its eigenspaces

$$V^\pm = \{\mathbf{A} \pm \mathcal{C}\mathbf{A} \mid \mathbf{A} \in L_t^2(S^2, \mathbb{C}^3)\} \quad (2.7)$$

corresponding to the eigenvalues ± 1 are orthogonal in $L_t^2(S^2, \mathbb{C}^3)$ and satisfy $L_t^2(S^2, \mathbb{C}^3) = V^+ \oplus V^-$. It has been shown in [16, 5] that

$$\begin{aligned} \mathbf{E}^i[\mathbf{A}] \text{ has helicity } \pm 1 & \quad \text{if and only if} & \quad \mathbf{A} \in V^\pm, \\ \mathbf{E}^s[\mathbf{A}]|_{\mathbb{R}^3 \setminus \bar{D}} \text{ has helicity } \pm 1 & \quad \text{if and only if} & \quad \mathbf{E}^\infty[\mathbf{A}] \in V^\pm. \end{aligned}$$

Electromagnetic chirality is a concept to describe the difference in the interaction of a scattering object D with incident fields of opposite helicities. To give an accurate definition, we denote by $\mathcal{P}^\pm : L_t^2(S^2, \mathbb{C}^3) \rightarrow L_t^2(S^2, \mathbb{C}^3)$ the orthogonal projections onto V^\pm , and accordingly we decompose

$$\mathcal{F}_D = \mathcal{F}_D^{++} + \mathcal{F}_D^{+-} + \mathcal{F}_D^{-+} + \mathcal{F}_D^{--} \quad (2.8)$$

with $\mathcal{F}_D^{pq} := \mathcal{P}^p \mathcal{F}_D \mathcal{P}^q$ for $p, q \in \{+, -\}$. It has been observed in [16, 5] that if a scatterer D is geometrically achiral, then there exists a unitary operator $\mathcal{U} : L_t^2(S^2, \mathbb{C}^3) \rightarrow L_t^2(S^2, \mathbb{C}^3)$ such that

$$\mathcal{C}\mathcal{U} = -\mathcal{U}\mathcal{C} \quad \text{and} \quad \mathcal{F}_D \mathcal{U} = \mathcal{U}\mathcal{F}_D.$$

This says that \mathcal{F}_D is equivalent to itself by means of a unitary transform \mathcal{U} that swaps helicity. An immediate consequence is that $\mathcal{F}_D^{++} = \mathcal{U}\mathcal{F}_D^{--}\mathcal{U}^*$ and $\mathcal{F}_D^{-+} = \mathcal{U}\mathcal{F}_D^{+-}\mathcal{U}^*$. Based on this observation, the following more general definition of electromagnetic chirality has been introduced in [16].

Definition 2.1. A scattering object D is called *electromagnetically achiral* (or *em-achiral*) if there exist unitary operators $\mathcal{U}^{(j)} : L_t^2(S^2, \mathbb{C}^3) \rightarrow L_t^2(S^2, \mathbb{C}^3)$ satisfying $\mathcal{U}^{(j)}\mathcal{C} = -\mathcal{C}\mathcal{U}^{(j)}$, $j = 1, \dots, 4$, such that

$$\mathcal{F}_D^{++} = \mathcal{U}^{(1)}\mathcal{F}_D^{--}\mathcal{U}^{(2)}, \quad \mathcal{F}_D^{-+} = \mathcal{U}^{(3)}\mathcal{F}_D^{+-}\mathcal{U}^{(4)}.$$

If this is not the case, we call the scattering object D *electromagnetically chiral* (or *em-chiral*).

An immediate consequence of this definition is that for an em-achiral scatterer D , the singular values (σ_j^{++}) of \mathcal{F}_D^{++} coincide with the singular values (σ_j^{--}) of \mathcal{F}_D^{--} and analogously the singular values (σ_j^{+-}) of \mathcal{F}_D^{+-} coincide with the singular values (σ_j^{-+}) of \mathcal{F}_D^{-+} . This leads to the idea of quantifying the degree of em-chirality of a scattering object by means of the distance of the corresponding sequences of singular values.

Following [16], we define the *chirality measure* χ_2 of a scatterer D associated to the far field operator \mathcal{F}_D as

$$\chi_2(\mathcal{F}_D) := (\|(\sigma_j^{++}) - (\sigma_j^{--})\|_{\ell^2}^2 + \|(\sigma_j^{+-}) - (\sigma_j^{-+})\|_{\ell^2}^2)^{\frac{1}{2}}. \quad (2.9)$$

Since the far field operator \mathcal{F}_D is an integral operator with smooth kernel, its singular values are decreasing exponentially and (2.9) is well-defined. In particular \mathcal{F}_D is a Hilbert-Schmidt operator. The chirality measure χ_2 is closely connected to the Hilbert-Schmidt norm of \mathcal{F}_D . In fact,

$$\chi_2(\mathcal{F}_D)^2 = \|\mathcal{F}_D\|_{\text{HS}}^2 - 2 \sum_j (\sigma_j^{++}\sigma_j^{--} + \sigma_j^{+-}\sigma_j^{-+}) \leq \|\mathcal{F}_D\|_{\text{HS}}^2, \quad (2.10)$$

and it follows immediately that the upper bound is attained, when $\mathcal{F}_D^{++} = \mathcal{F}_D^{-+} = 0$ or $\mathcal{F}_D^{--} = \mathcal{F}_D^{+-} = 0$, i.e., when the scatterer D does not scatter incident fields of either positive or negative helicity. If in addition the reciprocity principle holds, which is the case for the setting considered in this work (see, e.g., [13, Thm. 9.6]), then this invisibility property is known to be equivalent to equality in (2.10). The Hilbert-Schmidt norm $\|\mathcal{F}_D\|_{\text{HS}}$ of the far field operator is sometimes called the *total interaction cross-section* of the scattering object D .

Definition 2.2. A scattering object D is said to be *maximally em-chiral* if $\chi_2(\mathcal{F}_D) = \|\mathcal{F}_D\|_{\text{HS}}$.

Another possible choice for a chirality measures, which has been proposed in [22], is

$$\begin{aligned} \chi_{\text{HS}}(\mathcal{F}_D) &:= ((\|\mathcal{F}_D^{++}\|_{\text{HS}} - \|\mathcal{F}_D^{--}\|_{\text{HS}})^2 + (\|\mathcal{F}_D^{-+}\|_{\text{HS}} - \|\mathcal{F}_D^{+-}\|_{\text{HS}})^2)^{\frac{1}{2}} \\ &= (\|\mathcal{F}_D\|_{\text{HS}}^2 - 2(\|\mathcal{F}_D^{++}\|_{\text{HS}}\|\mathcal{F}_D^{--}\|_{\text{HS}} + \|\mathcal{F}_D^{-+}\|_{\text{HS}}\|\mathcal{F}_D^{+-}\|_{\text{HS}}))^{\frac{1}{2}}, \end{aligned} \quad (2.11)$$

Von Neumann's trace inequality (see, e.g., [15, lmm. XI.9.14]) shows that

$$\chi_{\text{HS}}(\mathcal{F}_D) \leq \chi_2(\mathcal{F}_D), \quad (2.12)$$

and comparing (2.10) and (2.11) we find that

$$\chi_{\text{HS}}(\mathcal{F}_D) = \|\mathcal{F}_D\|_{\text{HS}} \quad \text{if and only if} \quad \chi_2(\mathcal{F}_D) = \|\mathcal{F}_D\|_{\text{HS}}.$$

Moreover, χ_{HS} is differentiable on

$$X = \{\mathcal{G} \in \text{HS}(L_t^2(S^2, \mathbb{C}^3)) \mid \chi_{\text{HS}}(\mathcal{G}) \neq 0, \text{ and } \|\mathcal{G}^{pq}\|_{\text{HS}} > 0, p, q \in \{+, -\}\}, \quad (2.13)$$

where $\text{HS}(L_t^2(S^2, \mathbb{C}^3))$ denotes the space of Hilbert-Schmidt operators on $L_t^2(S^2, \mathbb{C}^3)$. Given $\mathcal{G} \in X$ and $\mathcal{H} \in \text{HS}(L_t^2(S^2, \mathbb{C}^3))$, the derivative is immediately seen to be given by

$$(\chi_{\text{HS}})'[\mathcal{G}]\mathcal{H} = \frac{\text{Re}\langle \mathcal{G}, \mathcal{H} \rangle_{\text{HS}} - \sum_{p,q \in \{+,-\}} \text{Re}\langle \mathcal{G}^{pq}, \mathcal{H}^{pq} \rangle_{\text{HS}} \frac{\|\mathcal{G}^{\bar{p}\bar{q}}\|_{\text{HS}}}{\|\mathcal{G}^{pq}\|_{\text{HS}}}}{\chi_{\text{HS}}(\mathcal{G})}, \quad (2.14)$$

where $\bar{p} := -p$ and $\bar{q} := -q$.

The remainder of this article is devoted to designing scatterers D that exhibit comparatively large values of $\chi_2(\mathcal{F}_D)$ and $\chi_{\text{HS}}(\mathcal{F}_D)$. Since numerical examples in [5] suggest that χ_2 is not differentiable, we use the chirality measure χ_{HS} in the gradient based shape optimization scheme that we develop in section 5 below. Furthermore, we will focus on thin tubular scattering objects, and in the next section we discuss an asymptotic representation formula for electric far field patterns due to such thin structures from [12] and apply it to our setting.

3 Far field operators of thin tubular scatterers

Before we specify the class of *thin tubular scattering objects* that will be considered in the following, we introduce a set of admissible parametrizations for the *center curves* of these scatterers by

$$\mathcal{U}_{\text{ad}} := \{\mathbf{p} \in C^3([0, 1], \mathbb{R}^3) \mid \mathbf{p}([0, 1]) \text{ is simple and } \mathbf{p}'(t) \neq 0 \text{ for all } t \in [0, 1]\}. \quad (3.1)$$

For any center curve $\Gamma \subseteq \mathbb{R}^3$ with parametrization $\mathbf{p}_\Gamma \in \mathcal{U}_{\text{ad}}$ we denote by $(\mathbf{t}_\Gamma, \mathbf{n}_\Gamma, \mathbf{b}_\Gamma)$ the corresponding Frenet-Serret frame. For instance, if $\mathbf{p}'_\Gamma(t) \times \mathbf{p}''_\Gamma(t) \neq 0$ for all $t \in [0, 1]$, then

$$\mathbf{t}_\Gamma = \frac{\mathbf{p}'_\Gamma}{|\mathbf{p}'_\Gamma|}, \quad \mathbf{n}_\Gamma = \frac{(\mathbf{p}'_\Gamma \times \mathbf{p}''_\Gamma) \times \mathbf{p}'_\Gamma}{|(\mathbf{p}'_\Gamma \times \mathbf{p}''_\Gamma) \times \mathbf{p}'_\Gamma|}, \quad \mathbf{b}_\Gamma = \mathbf{t}_\Gamma \times \mathbf{n}_\Gamma.$$

We will consider thin tubular scattering objects $D_\rho \subseteq \mathbb{R}^3$ with circular cross-section of radius $\rho > 0$, which are described by

$$D_\rho := \{\mathbf{p}_\Gamma(s) + \mathbf{n}_\Gamma(s)\eta + \mathbf{b}_\Gamma(s)\zeta \mid s \in (0, 1), |(\eta, \zeta)| < \rho\}. \quad (3.2)$$

In the following we assume that the parameter $\rho > 0$ is small with respect to the *wave length* $\lambda = 2\pi/k$ of the incident field, and that the relative electric permittivity and the relative magnetic permeability are given by

$$\varepsilon_{r, D_\rho}(\mathbf{x}) := \begin{cases} \varepsilon_r, & \mathbf{x} \in D_\rho, \\ 1, & \mathbf{x} \in \mathbb{R}^3 \setminus \overline{D_\rho}, \end{cases} \quad \text{and} \quad \mu_{r, D_\rho}(\mathbf{x}) := \begin{cases} \mu_r, & \mathbf{x} \in D_\rho, \\ 1, & \mathbf{x} \in \mathbb{R}^3 \setminus \overline{D_\rho}, \end{cases}$$

for some $\varepsilon_r, \mu_r > 0$. We denote the electric far field pattern of the solution to (2.1) with D replaced by D_ρ and a Herglotz incident field $\mathbf{E}^i[\mathbf{A}]$ by $\mathbf{E}_\rho^\infty[\mathbf{A}]$, and accordingly we write \mathcal{F}_{D_ρ} for the corresponding far field operator.

The computational complexity of the iterative shape optimization scheme developed in Section 5 below is heavily dominated by the evaluation of shape derivatives of far field operators corresponding to thin tubular scattering objects. We will facilitate these computations by incorporating the assumption that the scatterers are thin tubes directly into the model. To this end we apply the following asymptotic perturbation formula for the electric far field pattern \mathbf{E}_ρ^∞ as $\rho \rightarrow 0$, which has recently been established in [12] (see also [1, 19] and [3, 4, 8, 9, 10, 11] for earlier contributions in this direction).

Theorem 3.1. *Let $\Gamma \subseteq \mathbb{R}^3$ be an admissible center curve with $\mathbf{p}_\Gamma \in \mathcal{U}_{\text{ad}}$, and denote by $\varepsilon_r, \mu_r > 0$ the relative electric permittivity and the relative magnetic permittivity of a thin tubular scatterer D_ρ for some $\rho > 0$. Suppose that $\mathbf{A} \in L_t^2(S^2, \mathbb{C}^3)$ is the density of a Herglotz incident wave $\mathbf{E}^i[\mathbf{A}]$. Then the electric far field pattern of the corresponding solution to the scattering problem (2.1) satisfies, for each $\hat{\mathbf{x}} \in S^2$,*

$$\begin{aligned} \mathbf{E}_\rho^\infty[\mathbf{A}](\hat{\mathbf{x}}) &= (k\rho)^2 \pi \int_\Gamma \left((\varepsilon_r - 1) e^{-ik\hat{\mathbf{x}} \cdot \mathbf{y}} ((\hat{\mathbf{x}} \times \mathbb{I}_3) \times \hat{\mathbf{x}}) \mathbb{M}^\varepsilon(\mathbf{y}) \mathbf{E}^i[\mathbf{A}](\mathbf{y}) \right. \\ &\quad \left. + (\mu_r - 1) e^{-ik\hat{\mathbf{x}} \cdot \mathbf{y}} (\hat{\mathbf{x}} \times \mathbb{I}_3) \mathbb{M}^\mu(\mathbf{y}) \left(\frac{i}{k} \mathbf{curl} \mathbf{E}^i[\mathbf{A}](\mathbf{y}) \right) \right) ds(\mathbf{y}) + o((k\rho)^2) \end{aligned} \quad (3.3)$$

as $\rho \rightarrow 0$. The matrix valued functions $\mathbb{M}^\varepsilon, \mathbb{M}^\mu \in L^2(\Gamma, \mathbb{R}^{3 \times 3})$ are the so-called electric and magnetic polarization tensor, respectively. These are given by

$$\mathbb{M}^\gamma(\mathbf{p}_\Gamma(s)) = V_{\mathbf{p}_\Gamma}(s) M^\gamma V_{\mathbf{p}_\Gamma}(s)^\top \quad \text{for a.e. } s \in [0, 1] \text{ and } \gamma \in \{\varepsilon, \mu\},$$

where $M^\gamma := \text{diag}(1, 2/(\gamma_r + 1), 2/(\gamma_r + 1)) \in \mathbb{R}^{3 \times 3}$ and $V_{\mathbf{p}_\Gamma} := [\mathbf{t}_\Gamma \mid \mathbf{n}_\Gamma \mid \mathbf{b}_\Gamma] \in C([0, 1], \mathbb{C}^{3 \times 3})$ is the matrix valued function containing the components of the Frenet-Serret frame $(\mathbf{t}_\Gamma, \mathbf{n}_\Gamma, \mathbf{b}_\Gamma)$ for Γ as its columns.

Note that the cross product between a vector and a matrix in (3.3) denotes the matrix of cross products between the vector and the columns of the original matrix. The term $o((k\rho)^2)$ in (3.3) is such that $\|o((k\rho)^2)\|_{L^\infty(S^2)}/(k\rho)^2$ converges to zero for any fixed $\mathbf{E}^i[\mathbf{A}]$, and the dependence on $\mathbf{E}^i[\mathbf{A}]$ is only a dependence on $\|\mathbf{A}\|_{L_t^2(S^2, \mathbb{C}^3)}$.

Next we introduce the operator $\mathcal{T}_{D_\rho} : L_t^2(S^2, \mathbb{C}^3) \rightarrow L_t^2(S^2, \mathbb{C}^3)$, which is defined by

$$\begin{aligned} (\mathcal{T}_{D_\rho} \mathbf{A})(\hat{\mathbf{x}}) &:= (k\rho)^2 \pi \int_\Gamma \left((\varepsilon_r - 1) e^{-ik\hat{\mathbf{x}} \cdot \mathbf{y}} ((\hat{\mathbf{x}} \times \mathbb{I}_3) \times \hat{\mathbf{x}}) \mathbb{M}^\varepsilon(\mathbf{y}) \mathbf{E}^i[\mathbf{A}](\mathbf{y}) \right. \\ &\quad \left. + (\mu_r - 1) e^{-ik\hat{\mathbf{x}} \cdot \mathbf{y}} (\hat{\mathbf{x}} \times \mathbb{I}_3) \mathbb{M}^\mu(\mathbf{y}) \left(\frac{i}{k} \mathbf{curl} \mathbf{E}^i[\mathbf{A}](\mathbf{y}) \right) \right) ds(\mathbf{y}). \end{aligned} \quad (3.4)$$

From Theorem 3.1 (and the remark about the remainder term) it follows that

$$\mathcal{F}_{D_\rho} = \mathcal{T}_{D_\rho} + o((k\rho)^2) \quad \text{as } \rho \rightarrow 0, \quad (3.5)$$

and the term $o((k\rho)^2)$ in (3.5) is such that $\|o((k\rho)^2)\|_{\text{HS}}/(k\rho)^2$ converges to zero. Assuming that the radius $\rho > 0$ of the thin tubular scattering object D_ρ is sufficiently small with respect to the wave length of the incident fields, the last term on the right hand side of (3.5) can be neglected, and we may approximate the far field operator \mathcal{F}_{D_ρ} by \mathcal{T}_{D_ρ} .

For numerical implementations it will be convenient to have an explicit representation of \mathcal{T}_{D_ρ} in terms of a complete orthonormal system of $L_t^2(S^2, \mathbb{C}^3)$. Let $Y_n^m, m = -n, \dots, n, n \in \mathbb{N}$, denote any complete orthonormal system of spherical harmonics of order n in $L^2(S^2)$. A particular

choice that is used for the computations in our numerical examples is given in (A.2). Then, the *vector spherical harmonics*

$$\mathbf{U}_n^m(\boldsymbol{\theta}) = \frac{1}{\sqrt{n(n+1)}} \mathbf{Grad}_{S^2} Y_n^m(\boldsymbol{\theta}), \quad \mathbf{V}_n^m(\boldsymbol{\theta}) = \boldsymbol{\theta} \times \mathbf{U}_n^m(\boldsymbol{\theta}), \quad \boldsymbol{\theta} \in S^2, \quad (3.6)$$

for $m = -n, \dots, n, n = 1, 2, \dots$, form a complete orthonormal system in $L_t^2(S^2, \mathbb{C}^3)$. Accordingly we deduce that the *circularly polarized vector spherical harmonics*

$$\mathbf{A}_n^m := \frac{1}{\sqrt{2}}(\mathbf{U}_n^m + i\mathbf{V}_n^m) \quad \text{and} \quad \mathbf{B}_n^m := \frac{1}{\sqrt{2}}(\mathbf{U}_n^m - i\mathbf{V}_n^m), \quad (3.7)$$

for $m = -n, \dots, n, n = 1, 2, \dots$, form a complete orthonormal system in the subspace V^+ and V^- from (2.7), respectively. In particular,

$$i\boldsymbol{\theta} \times \mathbf{A}_n^m(\boldsymbol{\theta}) = \mathbf{A}_n^m(\boldsymbol{\theta}), \quad i\boldsymbol{\theta} \times \mathbf{B}_n^m(\boldsymbol{\theta}) = -\mathbf{B}_n^m(\boldsymbol{\theta}), \quad \boldsymbol{\theta} \in S^2. \quad (3.8)$$

We also consider the *spherical vector wave functions*

$$\mathbf{M}_n^m(\mathbf{x}) := -j_n(k|\mathbf{x}|)\mathbf{V}_n^m(\widehat{\mathbf{x}}), \quad \mathbf{x} \in \mathbb{R}^3, \quad m = -n, \dots, n, \quad n = 1, 2, 3, \dots, \quad (3.9)$$

where j_n denotes the spherical Bessel function of degree n . Note that the normalization factors used here differ from what is used elsewhere in the literature (see, e.g., [13, p. 255]). The corresponding Beltrami fields as defined in (2.6), which we will call *circularly polarized spherical vector wave functions* in the following, are given by

$$\mathbf{P}_n^m := \mathbf{M}_n^m + k^{-1} \mathbf{curl} \mathbf{M}_n^m, \quad \mathbf{Q}_n^m := \mathbf{M}_n^m - k^{-1} \mathbf{curl} \mathbf{M}_n^m \quad (3.10)$$

for $m = -n, \dots, n, n = 1, 2, \dots$. We recall that

$$\mathbf{curl} \mathbf{P}_n^m = k \mathbf{P}_n^m, \quad \mathbf{curl} \mathbf{Q}_n^m = -k \mathbf{Q}_n^m. \quad (3.11)$$

Lemma 3.2. *Let $\mathbf{A} \in L_t^2(S^2, \mathbb{C}^3)$ with*

$$\mathbf{A} = \sum_{n=1}^{\infty} \sum_{m=-n}^n (a_n^m \mathbf{A}_n^m + b_n^m \mathbf{B}_n^m). \quad (3.12)$$

Then

$$\mathcal{T}_{D_\rho} \mathbf{A} = \sum_{n=1}^{\infty} \sum_{m=-n}^n (c_n^m \mathbf{A}_n^m + d_n^m \mathbf{B}_n^m) \quad (3.13)$$

with

$$c_n^m = \sum_{n'=1}^{\infty} \sum_{m'=-n'}^{n'} \left(a_{n'}^{m'} \langle \mathcal{T}_{D_\rho} \mathbf{A}_{n'}^{m'}, \mathbf{A}_n^m \rangle_{L_t^2(S^2, \mathbb{C}^3)} + b_{n'}^{m'} \langle \mathcal{T}_{D_\rho} \mathbf{B}_{n'}^{m'}, \mathbf{A}_n^m \rangle_{L_t^2(S^2, \mathbb{C}^3)} \right), \quad (3.14a)$$

$$d_n^m = \sum_{n'=1}^{\infty} \sum_{m'=-n'}^{n'} \left(a_{n'}^{m'} \langle \mathcal{T}_{D_\rho} \mathbf{A}_{n'}^{m'}, \mathbf{B}_n^m \rangle_{L_t^2(S^2, \mathbb{C}^3)} + b_{n'}^{m'} \langle \mathcal{T}_{D_\rho} \mathbf{B}_{n'}^{m'}, \mathbf{B}_n^m \rangle_{L_t^2(S^2, \mathbb{C}^3)} \right). \quad (3.14b)$$

Introducing, for any $\mathbf{U}, \mathbf{V} \in C(\Gamma, \mathbb{C}^3)$, the expressions

$$\mathcal{J}^\pm(\mathbf{U}, \mathbf{V}) := 8\pi^3 k^2 \rho^2 \int_\Gamma \left(\pm(\varepsilon_r - 1) \overline{\mathbf{V}(\mathbf{y})} \cdot \mathbb{M}^\varepsilon(\mathbf{y}) \mathbf{U}(\mathbf{y}) + (\mu_r - 1) \overline{\mathbf{V}(\mathbf{y})} \cdot \mathbb{M}^\mu(\mathbf{y}) \mathbf{U}(\mathbf{y}) \right) ds(\mathbf{y}),$$

we have

$$\langle \mathcal{T}_{D_\rho} \mathbf{A}_{n'}^{m'}, \mathbf{A}_n^m \rangle_{L_t^2(S^2, \mathbb{C}^3)} = i^{n'-n} \mathcal{J}^+(\mathbf{P}_{n'}^{m'}(\mathbf{y}), \mathbf{P}_n^m(\mathbf{y})), \quad (3.15a)$$

$$\langle \mathcal{T}_{D_\rho} \mathbf{B}_{n'}^{m'}, \mathbf{A}_n^m \rangle_{L_t^2(S^2, \mathbb{C}^3)} = i^{n'-n} \mathcal{J}^-(\mathbf{Q}_{n'}^{m'}(\mathbf{y}), \mathbf{P}_n^m(\mathbf{y})), \quad (3.15b)$$

$$\langle \mathcal{T}_{D_\rho} \mathbf{A}_{n'}^{m'}, \mathbf{B}_n^m \rangle_{L_t^2(S^2, \mathbb{C}^3)} = i^{n'-n} \mathcal{J}^-(\mathbf{P}_{n'}^{m'}(\mathbf{y}), \mathbf{Q}_n^m(\mathbf{y})), \quad (3.15c)$$

$$\langle \mathcal{T}_{D_\rho} \mathbf{B}_{n'}^{m'}, \mathbf{B}_n^m \rangle_{L_t^2(S^2, \mathbb{C}^3)} = i^{n'-n} \mathcal{J}^+(\mathbf{Q}_{n'}^{m'}(\mathbf{y}), \mathbf{Q}_n^m(\mathbf{y})). \quad (3.15d)$$

Proof. The expansions (3.13) and (3.14) follow by linearity. Furthermore, it follows immediately from [13, thm. 6.29] that, for any $\boldsymbol{\theta} \in S^2$ and $\mathbf{p} \in \mathbb{C}^3$ with $\mathbf{p} \cdot \boldsymbol{\theta} = 0$,

$$\begin{aligned} \mathbf{p} e^{-ik\boldsymbol{\theta} \cdot \mathbf{y}} &= -4\pi \sum_{n=1}^{\infty} (-i)^n \sum_{m=-n}^n \overline{M_n^m(\mathbf{y})} (\mathbf{V}_n^m(\boldsymbol{\theta}) \cdot \mathbf{p}) \\ &\quad + \frac{4\pi}{k} \sum_{n=1}^{\infty} (-i)^{n-1} \sum_{m=-n}^n \overline{\mathbf{curl} M_n^m(\mathbf{y})} (\mathbf{U}_n^m(\boldsymbol{\theta}) \cdot \mathbf{p}). \end{aligned}$$

Hence, we find that

$$\langle e^{-ik\boldsymbol{\theta} \cdot \mathbf{y}}, \mathbf{U}_n^m(\boldsymbol{\theta}) \rangle_{L^2(S^2)} = \frac{4\pi}{k} (-i)^{n-1} \overline{\mathbf{curl} M_n^m(\mathbf{y})}, \quad (3.16a)$$

$$\langle e^{-ik\boldsymbol{\theta} \cdot \mathbf{y}}, \mathbf{V}_n^m(\boldsymbol{\theta}) \rangle_{L^2(S^2)} = -4\pi (-i)^n \overline{M_n^m(\mathbf{y})}, \quad (3.16b)$$

with the scalar product between a scalar and a vector understood to be taken componentwise, and recalling (3.7) and (3.10) this shows that

$$\langle e^{-ik\boldsymbol{\theta} \cdot \mathbf{y}}, \mathbf{A}_n^m(\boldsymbol{\theta}) \rangle_{L^2(S^2)} = \sqrt{8\pi} (-i)^{n-1} \overline{P_n^m(\mathbf{y})}, \quad (3.17a)$$

$$\langle e^{-ik\boldsymbol{\theta} \cdot \mathbf{y}}, \mathbf{B}_n^m(\boldsymbol{\theta}) \rangle_{L^2(S^2)} = -\sqrt{8\pi} (-i)^{n-1} \overline{Q_n^m(\mathbf{y})}. \quad (3.17b)$$

Therefore,

$$\mathbf{E}^i[\mathbf{A}_n^m] = \langle e^{ik\boldsymbol{\theta} \cdot \mathbf{y}}, \overline{\mathbf{A}_n^m(\boldsymbol{\theta})} \rangle_{L^2(S^2)} = \sqrt{8\pi} i^{n-1} P_n^m(\mathbf{y}), \quad (3.18a)$$

$$\mathbf{E}^i[\mathbf{B}_n^m] = \langle e^{ik\boldsymbol{\theta} \cdot \mathbf{y}}, \overline{\mathbf{B}_n^m(\boldsymbol{\theta})} \rangle_{L^2(S^2)} = -\sqrt{8\pi} i^{n-1} Q_n^m(\mathbf{y}), \quad (3.18b)$$

and applying (3.11) gives

$$\mathbf{curl} \mathbf{E}^i[\mathbf{A}_n^m] = \sqrt{8\pi} k i^{n-1} P_n^m(\mathbf{y}), \quad (3.19a)$$

$$\mathbf{curl} \mathbf{E}^i[\mathbf{B}_n^m] = \sqrt{8\pi} k i^{n-1} Q_n^m(\mathbf{y}). \quad (3.19b)$$

Similarly, applying (3.8) we obtain that

$$\langle e^{-ik\boldsymbol{\theta} \cdot \mathbf{y}} ((\boldsymbol{\theta} \times \mathbb{I}_3) \times \boldsymbol{\theta}), \mathbf{A}_n^m(\boldsymbol{\theta}) \rangle_{L_t^2(S^2, \mathbb{C}^3)} = \sqrt{8\pi} (-i)^{n-1} \overline{P_n^m(\mathbf{y})}^\top, \quad (3.20a)$$

$$\langle e^{-ik\boldsymbol{\theta} \cdot \mathbf{y}} ((\boldsymbol{\theta} \times \mathbb{I}_3) \times \boldsymbol{\theta}), \mathbf{B}_n^m(\boldsymbol{\theta}) \rangle_{L_t^2(S^2, \mathbb{C}^3)} = -\sqrt{8\pi} (-i)^{n-1} \overline{Q_n^m(\mathbf{y})}^\top, \quad (3.20b)$$

$$\langle e^{-ik\boldsymbol{\theta} \cdot \mathbf{y}} (\boldsymbol{\theta} \times \mathbb{I}_3), \mathbf{A}_n^m(\boldsymbol{\theta}) \rangle_{L_t^2(S^2, \mathbb{C}^3)} = \sqrt{8\pi} (-i)^n \overline{P_n^m(\mathbf{y})}^\top, \quad (3.20c)$$

$$\langle e^{-ik\boldsymbol{\theta} \cdot \mathbf{y}} (\boldsymbol{\theta} \times \mathbb{I}_3), \mathbf{B}_n^m(\boldsymbol{\theta}) \rangle_{L_t^2(S^2, \mathbb{C}^3)} = \sqrt{8\pi} (-i)^n \overline{Q_n^m(\mathbf{y})}^\top, \quad (3.20d)$$

with the scalar product between a matrix and a vector understood to be taken column by column. Finally, combining the identities in (3.16)–(3.20) with the integral representation in (3.4) gives (3.15). \square

Remark 3.3. The circularly polarized vector spherical harmonics \mathbf{A}_n^m and \mathbf{B}_n^m , $m = -n, \dots, n$, $n = 1, 2, \dots$, in (3.7) have been constructed in such a way that they span the subspaces V^+ and V^- from (2.7), respectively. Thus the expansion in lemma 3.2 immediately gives corresponding basis representations of the projected operators $\mathcal{T}_{D_\rho}^{pq}$ for $p, q \in \{+, -\}$, which are defined analogous to (2.8) with \mathcal{F}_{D_ρ} replaced by \mathcal{T}_{D_ρ} .

In numerical implementations the series over n in all these basis representations have to be truncated at some $N \in \mathbb{N}$. Studying the singular value decomposition of the linear operator that maps current densities supported in the ball $B_R(0)$ of radius R around the origin to their radiated far field patterns, it has been shown in [21] that for all practically relevant source distributions the radiated far field pattern is well approximated by a vector spherical harmonics expansion of order $N \gtrsim kR$. This suggests to choose the truncation index N in the series representations of \mathcal{T}_{D_ρ} and $\mathcal{T}_{D_\rho}^{pq}$, $p, q \in \{+, -\}$, such that $N \gtrsim kR$, where $B_R(0)$ denotes the smallest ball around the origin that contains the scattering object D_ρ . \diamond

4 The shape derivative of \mathcal{T}_{D_ρ}

In the previous section we have discussed the asymptotic behavior of the far field operator \mathcal{F}_{D_ρ} corresponding to a thin tubular scattering object D_ρ with circular cross-section of radius $\rho > 0$ and a fixed center curve Γ as ρ tends to zero. In this section we fix the radius $\rho > 0$ and discuss the Fréchet differentiability of the leading order term \mathcal{T}_{D_ρ} in the asymptotic expansion (3.5) with respect to the center curve Γ .

Recalling the set of admissible parametrizations \mathcal{U}_{ad} from (3.1), we define a non-linear operator $\mathbf{T}_\rho : \mathcal{U}_{\text{ad}} \rightarrow \text{HS}(L_t^2(S^2, \mathbb{C}^3))$ by

$$\mathbf{T}_\rho(\mathbf{p}_\Gamma) := \mathcal{T}_{D_\rho}, \quad (4.1)$$

where D_ρ is the thin tubular scattering object from (3.2) with center curve Γ parametrized by \mathbf{p}_Γ . Before we establish the Fréchet derivative of \mathbf{T}_ρ in theorem 4.2 below, we discuss the Fréchet differentiability of the polarization tensor \mathbb{M}^γ , $\gamma \in \{\mu, \varepsilon\}$, with respect to Γ . Recalling theorem 3.1 we can identify the parametrized form $\mathbb{M}_{\mathbf{p}_\Gamma}^\gamma := \mathbb{M}^\gamma \circ \mathbf{p}_\Gamma$ of the polarization tensor with a continuous function in $C([0, 1], \mathbb{R}^3)$. The following lemma has been established in [20, lmm. 4.1].

Lemma 4.1. *The mapping $\mathbf{p}_\Gamma \mapsto \mathbb{M}_{\mathbf{p}_\Gamma}^\gamma$ is Fréchet differentiable from \mathcal{U}_{ad} to $C([0, 1], \mathbb{C}^{3 \times 3})$, and its Fréchet derivative at $\mathbf{p}_\Gamma \in \mathcal{U}_{\text{ad}}$ is given by $\mathbf{h} \mapsto (\mathbb{M}_{\mathbf{p}_\Gamma, \mathbf{h}}^\gamma)'$ with*

$$(\mathbb{M}_{\mathbf{p}_\Gamma, \mathbf{h}}^\gamma)' = V_{\mathbf{p}_\Gamma, \mathbf{h}}' M^\gamma V_{\mathbf{p}_\Gamma}^\top + V_{\mathbf{p}_\Gamma} M^\gamma (V_{\mathbf{p}_\Gamma, \mathbf{h}}')^\top, \quad \mathbf{h} \in C^3([0, 1], \mathbb{R}^3),$$

where the matrix-valued function $V_{\mathbf{p}_\Gamma, \mathbf{h}}'$ is defined columnwise by

$$V_{\mathbf{p}_\Gamma, \mathbf{h}}' = \frac{1}{|\mathbf{p}_\Gamma'|} \left[(\mathbf{h}' \cdot \mathbf{n}_\Gamma) \mathbf{n}_\Gamma + (\mathbf{h}' \cdot \mathbf{b}_\Gamma) \mathbf{b}_\Gamma \mid - (\mathbf{h}' \cdot \mathbf{n}_\Gamma) \mathbf{t}_\Gamma \mid - (\mathbf{h}' \cdot \mathbf{b}_\Gamma) \mathbf{t}_\Gamma \right].$$

Next we establish the Fréchet differentiability of \mathbf{T}_ρ .

Theorem 4.2. *The operator \mathbf{T}_ρ is Fréchet differentiable and its Fréchet derivative at $\mathbf{p}_\Gamma \in \mathcal{U}_{\text{ad}}$ is given by $\mathbf{T}_\rho'[\mathbf{p}_\Gamma] : C^3([0, 1], \mathbb{R}^3) \rightarrow \text{HS}(L_t^2(S^2, \mathbb{C}^3))$ with*

$$\mathbf{T}_\rho'[\mathbf{p}_\Gamma] \mathbf{h} = (k\rho)^2 \pi \left((\varepsilon_r - 1) \sum_{j=1}^4 \mathbf{T}_{\rho, \varepsilon, j}'[\mathbf{p}_\Gamma] \mathbf{h} + (\mu_r - 1) \sum_{j=1}^4 \mathbf{T}_{\rho, \mu, j}'[\mathbf{p}_\Gamma] \mathbf{h} \right), \quad (4.2)$$

where, for any $\mathbf{A} \in L_t^2(S^2, \mathbb{C}^3)$,

$$((\mathbf{T}'_{\rho,\varepsilon,1}[\mathbf{p}_\Gamma]\mathbf{h})\mathbf{A})(\hat{\mathbf{x}}) = - \int_0^1 ik(\hat{\mathbf{x}} \cdot \mathbf{h}) e^{-ik\hat{\mathbf{x}} \cdot \mathbf{p}_\Gamma} ((\hat{\mathbf{x}} \times \mathbb{I}_3) \times \hat{\mathbf{x}}) \mathbb{M}_{\mathbf{p}_\Gamma}^\varepsilon \mathbf{E}^i[\mathbf{A}](\mathbf{p}_\Gamma) |\mathbf{p}'_\Gamma| dt, \quad (4.3a)$$

$$((\mathbf{T}'_{\rho,\varepsilon,2}[\mathbf{p}_\Gamma]\mathbf{h})\mathbf{A})(\hat{\mathbf{x}}) = \int_0^1 e^{-ik\hat{\mathbf{x}} \cdot \mathbf{p}_\Gamma} ((\hat{\mathbf{x}} \times \mathbb{I}_3) \times \hat{\mathbf{x}}) (\mathbb{M}_{\mathbf{p}_\Gamma, \mathbf{h}}^\varepsilon)' \mathbf{E}^i[\mathbf{A}](\mathbf{p}_\Gamma) |\mathbf{p}'_\Gamma| dt, \quad (4.3b)$$

$$((\mathbf{T}'_{\rho,\varepsilon,3}[\mathbf{p}_\Gamma]\mathbf{h})\mathbf{A})(\hat{\mathbf{x}}) = \int_0^1 e^{-ik\hat{\mathbf{x}} \cdot \mathbf{p}_\Gamma} ((\hat{\mathbf{x}} \times \mathbb{I}_3) \times \hat{\mathbf{x}}) \mathbb{M}_{\mathbf{p}_\Gamma}^\varepsilon (\mathbf{E}^i[\mathbf{A}])' [\mathbf{p}_\Gamma] \mathbf{h} |\mathbf{p}'_\Gamma| dt, \quad (4.3c)$$

$$((\mathbf{T}'_{\rho,\varepsilon,4}[\mathbf{p}_\Gamma]\mathbf{h})\mathbf{A})(\hat{\mathbf{x}}) = \int_0^1 e^{-ik\hat{\mathbf{x}} \cdot \mathbf{p}_\Gamma} ((\hat{\mathbf{x}} \times \mathbb{I}_3) \times \hat{\mathbf{x}}) \mathbb{M}_{\mathbf{p}_\Gamma}^\varepsilon \mathbf{E}^i[\mathbf{A}](\mathbf{p}_\Gamma) \frac{\mathbf{p}'_\Gamma \cdot \mathbf{h}'}{|\mathbf{p}'_\Gamma|} dt, \quad (4.3d)$$

and

$$((\mathbf{T}'_{\rho,\mu,1}[\mathbf{p}_\Gamma]\mathbf{h})\mathbf{A})(\hat{\mathbf{x}}) = - \int_0^1 ik(\hat{\mathbf{x}} \cdot \mathbf{h}) e^{-ik\hat{\mathbf{x}} \cdot \mathbf{p}_\Gamma} (\hat{\mathbf{x}} \times \mathbb{I}_3) \mathbb{M}_{\mathbf{p}_\Gamma}^\mu \left(\frac{i}{k} \mathbf{curl} \mathbf{E}^i[\mathbf{A}](\mathbf{p}_\Gamma) \right) |\mathbf{p}'_\Gamma| dt, \quad (4.4a)$$

$$((\mathbf{T}'_{\rho,\mu,2}[\mathbf{p}_\Gamma]\mathbf{h})\mathbf{A})(\hat{\mathbf{x}}) = \int_0^1 e^{-ik\hat{\mathbf{x}} \cdot \mathbf{p}_\Gamma} (\hat{\mathbf{x}} \times \mathbb{I}_3) (\mathbb{M}_{\mathbf{p}_\Gamma, \mathbf{h}}^\mu)' \left(\frac{i}{k} \mathbf{curl} \mathbf{E}^i[\mathbf{A}](\mathbf{p}_\Gamma) \right) |\mathbf{p}'_\Gamma| dt, \quad (4.4b)$$

$$((\mathbf{T}'_{\rho,\mu,3}[\mathbf{p}_\Gamma]\mathbf{h})\mathbf{A})(\hat{\mathbf{x}}) = \int_0^1 e^{-ik\hat{\mathbf{x}} \cdot \mathbf{p}_\Gamma} (\hat{\mathbf{x}} \times \mathbb{I}_3) \mathbb{M}_{\mathbf{p}_\Gamma}^\mu \left(\frac{i}{k} \mathbf{curl} \mathbf{E}^i[\mathbf{A}] \right)' [\mathbf{p}_\Gamma] \mathbf{h} |\mathbf{p}'_\Gamma| dt, \quad (4.4c)$$

$$((\mathbf{T}'_{\rho,\mu,4}[\mathbf{p}_\Gamma]\mathbf{h})\mathbf{A})(\hat{\mathbf{x}}) = \int_0^1 e^{-ik\hat{\mathbf{x}} \cdot \mathbf{p}_\Gamma} (\hat{\mathbf{x}} \times \mathbb{I}_3) \mathbb{M}_{\mathbf{p}_\Gamma}^\mu \left(\frac{i}{k} \mathbf{curl} \mathbf{E}^i[\mathbf{A}](\mathbf{p}_\Gamma) \right) \frac{\mathbf{p}'_\Gamma \cdot \mathbf{h}'}{|\mathbf{p}'_\Gamma|} dt. \quad (4.4d)$$

Proof. Let $\mathbf{p}_\Gamma \in \mathcal{U}_{\text{ad}}$, then there exists $\delta > 0$ such that $\mathbf{p}_\Gamma + \mathbf{h} \in \mathcal{U}_{\text{ad}}$ for all $\mathbf{h} \in C^3([0, 1], \mathbb{R}^3)$ satisfying $\|\mathbf{h}\|_{C^3([0,1], \mathbb{R}^3)} \leq \delta$. We have to show that

$$\|\mathbf{T}_\rho(\mathbf{p}_\Gamma + \mathbf{h}) - \mathbf{T}_\rho(\mathbf{p}_\Gamma) - \mathbf{T}'_\rho[\mathbf{p}_\Gamma]\mathbf{h}\|_{\text{HS}} = o(\|\mathbf{h}\|_{C^3([0,1], \mathbb{R}^3)}) \quad \text{as } \|\mathbf{h}\|_{C^3([0,1], \mathbb{R}^3)} \rightarrow 0. \quad (4.5)$$

Using (3.4), (4.2)–(4.4) and (2.3), the Hilbert-Schmidt operators $\mathbf{T}_\rho(\mathbf{p}_\Gamma + \mathbf{h})$, $\mathbf{T}_\rho(\mathbf{p}_\Gamma)$, and $\mathbf{T}'_\rho[\mathbf{p}_\Gamma]\mathbf{h}$ can be written as integral operators such that, for any $\mathbf{A} \in L_t^2(S^2, \mathbb{C}^3)$,

$$\begin{aligned} (\mathbf{T}_\rho(\mathbf{p}_\Gamma + \mathbf{h})\mathbf{A})(\hat{\mathbf{x}}) &= \int_{S^2} K_{\mathbf{p}_\Gamma + \mathbf{h}}(\hat{\mathbf{x}}, \boldsymbol{\theta}) \mathbf{A}(\boldsymbol{\theta}) ds(\boldsymbol{\theta}), \\ (\mathbf{T}_\rho(\mathbf{p}_\Gamma)\mathbf{A})(\hat{\mathbf{x}}) &= \int_{S^2} K_{\mathbf{p}_\Gamma}(\hat{\mathbf{x}}, \boldsymbol{\theta}) \mathbf{A}(\boldsymbol{\theta}) ds(\boldsymbol{\theta}), \\ ((\mathbf{T}'_\rho[\mathbf{p}_\Gamma]\mathbf{h})\mathbf{A})(\hat{\mathbf{x}}) &= \int_{S^2} K'_{\mathbf{p}_\Gamma, \mathbf{h}}(\hat{\mathbf{x}}, \boldsymbol{\theta}) \mathbf{A}(\boldsymbol{\theta}) ds(\boldsymbol{\theta}), \end{aligned}$$

with smooth kernels $K_{\mathbf{p}_\Gamma + \mathbf{h}}$, $K_{\mathbf{p}_\Gamma}$ and $K'_{\mathbf{p}_\Gamma, \mathbf{h}}$ in $L^2(S^2 \times S^2, \mathbb{C}^{3 \times 3})$. Using the complete orthonormal system of vector spherical harmonics from (3.6) we obtain that

$$\begin{aligned} &\|\mathbf{T}_\rho(\mathbf{p}_\Gamma + \mathbf{h}) - \mathbf{T}_\rho(\mathbf{p}_\Gamma) - \mathbf{T}'_\rho[\mathbf{p}_\Gamma]\mathbf{h}\|_{\text{HS}}^2 \\ &= \sum_{n=1}^{\infty} \sum_{m=-n}^n \left(\|(\mathbf{T}_\rho(\mathbf{p}_\Gamma + \mathbf{h}) - \mathbf{T}_\rho(\mathbf{p}_\Gamma) - \mathbf{T}'_\rho[\mathbf{p}_\Gamma]\mathbf{h}) \mathbf{U}_n^m\|_{L_t^2(S^2, \mathbb{C}^3)}^2 \right. \\ &\quad \left. + \|(\mathbf{T}_\rho(\mathbf{p}_\Gamma + \mathbf{h}) - \mathbf{T}_\rho(\mathbf{p}_\Gamma) - \mathbf{T}'_\rho[\mathbf{p}_\Gamma]\mathbf{h}) \mathbf{V}_n^m\|_{L_t^2(S^2, \mathbb{C}^3)}^2 \right) \\ &= \int_{S^2} \sum_{n=1}^{\infty} \sum_{m=-n}^n \left(\left| \int_{S^2} (K_{\mathbf{p}_\Gamma + \mathbf{h}} - K_{\mathbf{p}_\Gamma} - K'_{\mathbf{p}_\Gamma, \mathbf{h}})(\boldsymbol{\theta}, \hat{\mathbf{x}}) \mathbf{U}_n^m(\hat{\mathbf{x}}) ds(\hat{\mathbf{x}}) \right|^2 ds(\boldsymbol{\theta}) \right. \\ &\quad \left. + \left| \int_{S^2} (K_{\mathbf{p}_\Gamma + \mathbf{h}} - K_{\mathbf{p}_\Gamma} - K'_{\mathbf{p}_\Gamma, \mathbf{h}})(\boldsymbol{\theta}, \hat{\mathbf{x}}) \mathbf{V}_n^m(\hat{\mathbf{x}}) ds(\hat{\mathbf{x}}) \right|^2 ds(\boldsymbol{\theta}) \right). \end{aligned} \quad (4.6)$$

Thus, Parseval's identity shows that

$$\begin{aligned} & \left\| \mathbf{T}_\rho(\mathbf{p}_\Gamma + \mathbf{h}) - \mathbf{T}_\rho(\mathbf{p}_\Gamma) - \mathbf{T}'_\rho[\mathbf{p}_\Gamma]\mathbf{h} \right\|_{\text{HS}}^2 \\ &= \int_{S^2} \int_{S^2} \left\| (K_{\mathbf{p}_\Gamma + \mathbf{h}} - K_{\mathbf{p}_\Gamma} - K'_{\mathbf{p}_\Gamma, \mathbf{h}})(\boldsymbol{\theta}, \hat{\mathbf{x}}) \right\|_F^2 ds(\boldsymbol{\theta}) ds(\hat{\mathbf{x}}), \end{aligned} \quad (4.7)$$

where $\|\cdot\|_F$ denotes the Frobenius norm on $\mathbb{C}^{3 \times 3}$. Proceeding as in the proof of [20, thm. 4.2], applying Taylor's theorem, it is straightforward to show that

$$\int_{S^2} \int_{S^2} \left\| (K_{\mathbf{p}_\Gamma + \mathbf{h}} - K_{\mathbf{p}_\Gamma} - K'_{\mathbf{p}_\Gamma, \mathbf{h}})(\boldsymbol{\theta}, \hat{\mathbf{x}}) \right\|_F^2 ds(\boldsymbol{\theta}) ds(\hat{\mathbf{x}}) \leq C \|\mathbf{h}\|_{\mathbb{C}^3([0,1], \mathbb{R}^3)}^4.$$

Together with (4.7) this implies (4.5). \square

As already done for \mathcal{T}_{D_ρ} in Lemma 3.2, we next derive an explicit basis representation of the Fréchet derivative $\mathbf{T}'_\rho[\mathbf{p}_\Gamma]\mathbf{h}$ in terms of the circularly polarized vector spherical harmonics \mathbf{A}_n^m and \mathbf{B}_n^m , $m = -n, \dots, n$, $n = 1, 2, \dots$ from (3.7).

Remark 4.3. Let $\mathbf{A} \in L_t^2(S^2, \mathbb{C}^3)$ with

$$\mathbf{A} = \sum_{n=1}^{\infty} \sum_{m=-n}^n (a_n^m \mathbf{A}_n^m + b_n^m \mathbf{B}_n^m). \quad (4.8)$$

Then

$$(\mathbf{T}'_\rho[\mathbf{p}_\Gamma]\mathbf{h})\mathbf{A} = \sum_{n=1}^{\infty} \sum_{m=-n}^n (c_n^m \mathbf{A}_n^m + d_n^m \mathbf{B}_n^m) \quad (4.9)$$

with

$$c_n^m = \sum_{n'=1}^{\infty} \sum_{m'=-n'}^{n'} \left(a_{n'}^{m'} \langle (\mathbf{T}'_\rho[\mathbf{p}_\Gamma]\mathbf{h})\mathbf{A}_{n'}^{m'}, \mathbf{A}_n^m \rangle_{L_t^2(S^2, \mathbb{C}^3)} + b_{n'}^{m'} \langle (\mathbf{T}'_\rho[\mathbf{p}_\Gamma]\mathbf{h})\mathbf{B}_{n'}^{m'}, \mathbf{A}_n^m \rangle_{L_t^2(S^2, \mathbb{C}^3)} \right), \quad (4.10a)$$

$$d_n^m = \sum_{n'=1}^{\infty} \sum_{m'=-n'}^{n'} \left(a_{n'}^{m'} \langle (\mathbf{T}'_\rho[\mathbf{p}_\Gamma]\mathbf{h})\mathbf{A}_{n'}^{m'}, \mathbf{B}_n^m \rangle_{L_t^2(S^2, \mathbb{C}^3)} + b_{n'}^{m'} \langle (\mathbf{T}'_\rho[\mathbf{p}_\Gamma]\mathbf{h})\mathbf{B}_{n'}^{m'}, \mathbf{B}_n^m \rangle_{L_t^2(S^2, \mathbb{C}^3)} \right). \quad (4.10b)$$

The inner products in (4.10) can be evaluated using (4.3)–(4.4), and the identities (3.18)–(3.20) as well as

$$\begin{aligned} (\mathbf{E}^i[\mathbf{A}_n^m])'[\mathbf{y}] &= \sqrt{8\pi} i^{n-1} (\mathbf{P}_n^m)'[\mathbf{y}], \\ (\mathbf{E}^i[\mathbf{B}_n^m])'[\mathbf{y}] &= -\sqrt{8\pi} i^{n-1} (\mathbf{Q}_n^m)'[\mathbf{y}], \end{aligned}$$

and

$$\begin{aligned} (\mathbf{curl} \mathbf{E}^i[\mathbf{A}_n^m])'[\mathbf{y}] &= \sqrt{8\pi} k i^{n-1} (\mathbf{P}_n^m)'[\mathbf{y}], \\ (\mathbf{curl} \mathbf{E}^i[\mathbf{B}_n^m])'[\mathbf{y}] &= \sqrt{8\pi} k i^{n-1} (\mathbf{Q}_n^m)'[\mathbf{y}], \end{aligned}$$

and

$$\begin{aligned} \langle ik(\hat{\mathbf{x}} \cdot \mathbf{h}) e^{-ik\hat{\mathbf{x}} \cdot \mathbf{y}} ((\hat{\mathbf{x}} \times \mathbb{I}_3) \times \hat{\mathbf{x}}), \mathbf{A}_n^m(\hat{\mathbf{x}}) \rangle_{L_t^2(S^2, \mathbb{C}^3)} &= \sqrt{8\pi} (-i)^{n-1} \overline{(\mathbf{P}_n^m)'[\mathbf{y}] \mathbf{h}^\top}, \\ \langle ik(\hat{\mathbf{x}} \cdot \mathbf{h}) e^{-ik\hat{\mathbf{x}} \cdot \mathbf{y}} ((\hat{\mathbf{x}} \times \mathbb{I}_3) \times \hat{\mathbf{x}}), \mathbf{B}_n^m(\hat{\mathbf{x}}) \rangle_{L_t^2(S^2, \mathbb{C}^3)} &= -\sqrt{8\pi} (-i)^{n-1} \overline{(\mathbf{Q}_n^m)'[\mathbf{y}] \mathbf{h}^\top}, \\ \langle ik(\hat{\mathbf{x}} \cdot \mathbf{h}) e^{-ik\hat{\mathbf{x}} \cdot \mathbf{y}} (\hat{\mathbf{x}} \times \mathbb{I}_3), \mathbf{A}_n^m(\hat{\mathbf{x}}) \rangle_{L_t^2(S^2, \mathbb{C}^3)} &= \sqrt{8\pi} (-i)^n \overline{(\mathbf{P}_n^m)'[\mathbf{y}] \mathbf{h}^\top}, \\ \langle ik(\hat{\mathbf{x}} \cdot \mathbf{h}) e^{-ik\hat{\mathbf{x}} \cdot \mathbf{y}} (\hat{\mathbf{x}} \times \mathbb{I}_3), \mathbf{B}_n^m(\hat{\mathbf{x}}) \rangle_{L_t^2(S^2, \mathbb{C}^3)} &= \sqrt{8\pi} (-i)^n \overline{(\mathbf{Q}_n^m)'[\mathbf{y}] \mathbf{h}^\top}. \end{aligned}$$

Explicit formulas for the derivatives $(\mathbf{P}_n^m)'$ and $(\mathbf{Q}_n^m)'$ of the circularly polarized spherical vector wave functions \mathbf{P}_n^m and \mathbf{Q}_n^m , $m = -n, \dots, n$, $n = 1, 2, \dots$, from (3.10) can be found in Appendix A. \diamond

5 Shape optimization for thin em-chiral structures

We develop a shape optimization scheme to determine dielectric thin tubular scattering objects D_ρ as in (3.2) that exhibit comparatively large measures of em-chirality χ_{HS} at a given frequency. In addition to the frequency, we also fix the material parameters ε_r, μ_r and the length $|\Gamma|$ of the center curve Γ of D_ρ before we start the optimization process. Furthermore, we assume that the radius $\rho > 0$ of the circular cross-section of D_ρ is sufficiently small with respect to the wave length of the incident fields, such that the leading order term \mathcal{T}_{D_ρ} in the asymptotic expansion (3.5) gives a good approximation of the far field operator \mathcal{F}_{D_ρ} .

Combining (2.10) and (2.12) we find that

$$0 \leq \chi_{\text{HS}}(\mathcal{G}) \leq \|\mathcal{G}\|_{\text{HS}}^2 \quad \text{for any } \mathcal{G} \in \text{HS}(L_t^2(S^2, \mathbb{C}^3)).$$

Accordingly, recalling the definition of the non-linear operator \mathbf{T}_ρ in (4.1), we normalize the chirality measure χ_{HS} and consider the bounded *objective functional* $J_{\text{HS}} : \mathcal{U}_{\text{ad}} \rightarrow [0, 1]$, which is given by

$$J_{\text{HS}}(\mathbf{p}_\Gamma) := \frac{\chi_{\text{HS}}(\mathbf{T}_\rho(\mathbf{p}_\Gamma))}{\|\mathbf{T}_\rho(\mathbf{p}_\Gamma)\|_{\text{HS}}}. \quad (5.1)$$

We discuss the optimization problem

$$\text{find } \arg \min_{\mathbf{p}_\Gamma \in \mathcal{U}_{\text{ad}}} (-J_{\text{HS}}(\mathbf{p}_\Gamma)) \quad \text{subject to } |\Gamma| = L \quad (5.2)$$

for some prescribed length $L > 0$.

Remark 5.1. Since the leading order term in the asymptotic expansion of the electric far field pattern due to a thin tubular scattering object in (3.3) is homogeneous of degree two with respect to the radius ρ of the cross-section of the scatterer D_ρ , the same is true for $\mathbf{T}_\rho(\mathbf{p}_\Gamma)$ as well as for $\chi_{\text{HS}}(\mathbf{T}_\rho(\mathbf{p}_\Gamma))$ and $\|\mathbf{T}_\rho(\mathbf{p}_\Gamma)\|_{\text{HS}}$ with $\mathbf{p}_\Gamma \in \mathcal{U}_{\text{ad}}$. In particular the relative chirality measure $J_{\text{HS}}(\mathbf{p}_\Gamma)$ and thus also (local) minimizers for (5.2) are independent of ρ . \diamond

Below we rewrite (5.2) as an unconstrained optimization problem and apply a quasi-Newton method to approximate a (local) minimizer. This requires the Fréchet derivative of the objective functional J_{HS} , which is for any $\mathbf{p}_\Gamma \in \mathcal{U}_{\text{ad}}$ such that $\mathbf{T}_\rho(\mathbf{p}_\Gamma) \in X$, where the space X has been introduced in (2.13), and for any $\mathbf{h} \in C^3([0, 1], \mathbb{R}^3)$ given by

$$J'_{\text{HS}}[\mathbf{p}_\Gamma]\mathbf{h} = \frac{(\chi_{\text{HS}})'[\mathbf{T}_\rho(\mathbf{p}_\Gamma)](\mathbf{T}'_\rho[\mathbf{p}_\Gamma]\mathbf{h})}{\|\mathbf{T}_\rho(\mathbf{p}_\Gamma)\|_{\text{HS}}} - \frac{\chi_{\text{HS}}[\mathbf{T}_\rho(\mathbf{p}_\Gamma)] \text{Re}\langle \mathbf{T}_\rho(\mathbf{p}_\Gamma), \mathbf{T}'_\rho[\mathbf{p}_\Gamma]\mathbf{h} \rangle_{\text{HS}}}{\|\mathbf{T}_\rho(\mathbf{p}_\Gamma)\|_{\text{HS}}^3}.$$

The Fréchet derivatives $(\chi_{\text{HS}})'$ and \mathbf{T}'_ρ have already been established in (2.14) and in theorem 4.2, respectively.

5.1 Discretization and regularization

In the numerical implementation of the optimization algorithm we approximate admissible center curves Γ of thin tubular scatterers D_ρ using interpolating cubic splines with the not-a-knot condition at the end points. We consider a partition

$$\Delta := \{0 = t_1 < t_2 < \dots < t_n = 1\} \subseteq [0, 1],$$

and denote the not-a-knot spline that interpolates the curve Γ with parametrization $\mathbf{p}_\Gamma \in \mathcal{U}_{\text{ad}}$ at the knots $\mathbf{x}^{(j)} = \mathbf{p}_\Gamma(t_j)$, $j = 1, \dots, n$, by $\mathbf{p}_\Delta[\vec{\mathbf{x}}]$, where $\vec{\mathbf{x}} \in \mathbb{R}^{3n}$ is the vector that contains the coordinates of the control points $\mathbf{x}^{(1)}, \dots, \mathbf{x}^{(n)}$. The space of all not-a-knot splines with respect to Δ is denoted by $\mathcal{P}_\Delta \not\subseteq \mathcal{U}_{\text{ad}}$.

To stabilize the optimization procedure, and to incorporate the constraint in (5.2), we include two penalty terms into the objective functional. The total squared curvature functional $\Psi_1 : \mathcal{P}_\Delta \rightarrow \mathbb{R}$ is defined by

$$\Psi_1(\mathbf{p}_\Delta) := \int_0^1 \kappa^2(s) |\mathbf{p}'_\Delta(s)| \, ds,$$

where

$$\kappa(s) := \frac{|\mathbf{p}'_\Delta(s) \times \mathbf{p}''_\Delta(s)|}{|\mathbf{p}'_\Delta(s)|^3} = \frac{1}{|\mathbf{p}'_\Delta|} \left| \frac{\mathbf{p}''_\Delta}{|\mathbf{p}'_\Delta|} - \frac{\mathbf{p}'_\Delta \cdot \mathbf{p}''_\Delta}{|\mathbf{p}'_\Delta|^3} \mathbf{p}'_\Delta \right|, \quad s \in [0, 1],$$

denotes the curvature of the curve Γ that is parametrized by \mathbf{p}_Δ . Adding $\alpha_1 \Psi_1$ with a suitable regularization parameter $\alpha_1 > 0$ as a penalty term to $-J_{\text{HS}}$ prevents minimizers from being too strongly entangled.

Furthermore, we define $\Psi_2 : \mathcal{P}_\Delta \rightarrow \mathbb{R}$ by

$$\Psi_2(\mathbf{p}_\Delta) := \sum_{j=1}^{n-1} \left| \frac{L}{n-1} - \int_{t_j}^{t_{j+1}} |\mathbf{p}'_\Delta(s)| \, ds \right|^2.$$

We add $\alpha_2 \Psi_2$ with a suitable regularization parameter $\alpha_2 > 0$ as a penalty term to $-J_{\text{HS}} + \alpha_1 \Psi_1$ to enforce the constraint $|\Gamma| = L$ in (5.2), and to promote uniformly distributed control points along the spline approximation of Γ during the minimization process.

Altogether, we obtain the regularized discrete nonlinear objective functional $\Phi : \mathcal{P}_\Delta \rightarrow \mathbb{R}$,

$$\Phi(\mathbf{p}_\Delta) := -J_{\text{HS}}(\mathbf{p}_\Delta) + \alpha_1 \Psi_1(\mathbf{p}_\Delta) + \alpha_2 \Psi_2(\mathbf{p}_\Delta), \quad (5.3)$$

and we consider the unconstrained optimization problem

$$\text{find } \mathbf{p}_\Delta^* := \arg \min_{\mathbf{p}_\Delta \in \mathcal{P}_\Delta} \Phi(\mathbf{p}_\Delta). \quad (5.4)$$

Before we describe the quasi-Newton optimization scheme, we discuss the Fréchet derivatives of the functionals Ψ_1 and Ψ_2 . A short calculation gives the following result.

Lemma 5.2. *The mappings Ψ_1 and Ψ_2 are Fréchet differentiable from $\mathcal{P}_\Delta \subseteq C^2([0, 1], \mathbb{R}^3)$ to \mathbb{R} . Their Fréchet derivatives at $\mathbf{p}_\Delta \in \mathcal{P}_\Delta$ are given by $\Psi'_1[\mathbf{p}_\Delta] : \mathcal{P}_\Delta \rightarrow \mathbb{R}$ with*

$$\begin{aligned} \Psi'_1[\mathbf{p}_\Delta] \mathbf{h}_\Delta = \int_0^1 & \left(2 \frac{\mathbf{p}''_\Delta \cdot \mathbf{h}''_\Delta}{|\mathbf{p}'_\Delta|^3} - 3 \frac{|\mathbf{p}''_\Delta|^2 (\mathbf{p}'_\Delta \cdot \mathbf{h}'_\Delta)}{|\mathbf{p}'_\Delta|^5} \right. \\ & \left. - 2 \frac{(\mathbf{p}'_\Delta \cdot \mathbf{h}''_\Delta + \mathbf{p}''_\Delta \cdot \mathbf{h}'_\Delta) (\mathbf{p}'_\Delta \cdot \mathbf{p}''_\Delta)}{|\mathbf{p}'_\Delta|^5} + 5 \frac{(\mathbf{p}'_\Delta \cdot \mathbf{h}'_\Delta) (\mathbf{p}'_\Delta \cdot \mathbf{p}''_\Delta)^2}{|\mathbf{p}'_\Delta|^7} \right) ds, \end{aligned}$$

and $\Psi'_2[\mathbf{p}_\Delta] : \mathcal{P}_\Delta \rightarrow \mathbb{R}$ with

$$\Psi'_2[\mathbf{p}_\Delta] \mathbf{h}_\Delta = -2 \sum_{j=1}^{n-1} \left(\int_{t_j}^{t_{j+1}} \frac{\mathbf{p}'_\Delta \cdot \mathbf{h}'_\Delta}{|\mathbf{p}'_\Delta|} \, ds \right) \left(\frac{L}{n-1} - \int_{t_j}^{t_{j+1}} |\mathbf{p}'_\Delta| \, ds \right).$$

5.2 The BFGS scheme for the regularized optimization problem

We apply a BFGS scheme with an inexact Armijo-type line search and a cautious update rule as described in [27] to approximate a solution to (5.4).

Choosing an initial guess $\vec{\mathbf{x}}_0$ for the coordinates of the control points of the center spline $\mathbf{p}_\Delta[\vec{\mathbf{x}}_0]$, the BFGS iteration for (5.4) is given by

$$\vec{\mathbf{x}}_{\ell+1} = \vec{\mathbf{x}}_\ell + \lambda_\ell \mathbf{d}_\ell, \quad \ell = 0, 1, \dots, \quad (5.5)$$

where \mathbf{d}_ℓ is obtained by solving the linear system

$$H_\ell \mathbf{d}_\ell = -\nabla \Phi(\mathbf{p}_\Delta[\vec{\mathbf{x}}_\ell]),$$

and H_ℓ is an approximation to the Hessian matrix $\nabla^2 \Phi(\mathbf{p}_\Delta[\vec{\mathbf{x}}_\ell])$.

We start with $H_0 = \mathbb{I}_{3n}$, and after each iteration we use the cautious update rule from [27], which is given by

$$H_{\ell+1} = \begin{cases} H_\ell - \frac{H_\ell \mathbf{s}_\ell \mathbf{s}_\ell^\top H_\ell}{\mathbf{s}_\ell^\top H_\ell \mathbf{s}_\ell} + \frac{\mathbf{y}_\ell \mathbf{y}_\ell^\top}{\mathbf{y}_\ell^\top \mathbf{s}_\ell} & \text{if } \frac{\mathbf{y}_\ell^\top \mathbf{s}_\ell}{|\mathbf{s}_\ell|^2} > \varepsilon |\nabla \Phi(\mathbf{p}_\Delta[\vec{\mathbf{x}}_\ell])|, \\ H_\ell & \text{otherwise,} \end{cases} \quad (5.6)$$

where

$$\mathbf{s}_\ell := \vec{\mathbf{x}}_{\ell+1} - \vec{\mathbf{x}}_\ell, \quad \mathbf{y}_\ell := \nabla \Phi(\mathbf{p}_\Delta[\vec{\mathbf{x}}_{\ell+1}]) - \nabla \Phi(\mathbf{p}_\Delta[\vec{\mathbf{x}}_\ell]),$$

and $\varepsilon > 0$ is a parameter. This ensures positive definiteness of H_ℓ throughout the iteration (cf. [27]).

As suggested in [27], we use an inexact Armijo-type line search to determine the step size λ_ℓ in (5.5). Choosing parameters $\sigma \in (0, 1)$ and $\delta \in (0, 1)$, we identify the smallest integer $j = 0, 1, \dots$, such that δ^j satisfies

$$\Phi(\mathbf{p}_\Delta[\vec{\mathbf{x}}_\ell] + \delta^j \mathbf{d}_\ell) \leq \Phi(\mathbf{p}_\Delta[\vec{\mathbf{x}}_\ell]) + \sigma \delta^j \nabla \Phi(\mathbf{p}_\Delta[\vec{\mathbf{x}}_\ell])^\top \mathbf{d}_\ell. \quad (5.7)$$

Then we set $\lambda_\ell = \delta^j$.

In the numerical examples presented in section 6 below, we use the parameters $\varepsilon = 10^{-5}$, $\sigma = 10^{-4}$, and $\delta = 0.9$ in (5.6) and (5.7). Denoting by $N \in \mathbb{N}$ be the maximal degree of vector spherical harmonics that are used in the basis representation of the operators $\mathbf{T}_\rho(\mathbf{p}_\Delta)$ (see lemma 3.2) and $\mathbf{T}'_\rho[\mathbf{p}_\Delta] \mathbf{h}$ (see remark 4.3), we consider discrete approximations $\mathbf{T}_{\rho, N}(\mathbf{p}_\Delta) \in \mathbb{C}^{Q \times Q}$ and $\mathbf{T}'_{\rho, N}[\mathbf{p}_\Delta] \mathbf{h} \in \mathbb{C}^{Q \times Q}$ with $Q = 2N(N+2)$. We approximate the integrals over the parameter range $[0, 1]$ of the spline $\mathbf{p}_\Delta[\vec{\mathbf{x}}_\ell]$ in the evaluation of $\nabla \Phi(\mathbf{p}_\Delta[\vec{\mathbf{x}}_\ell])$, $\ell = 0, 1, \dots$, using a composite Simpson's rule with $M = 5$ nodes on each subinterval of the partition Δ . We stop the BFGS iteration when $|\vec{\mathbf{x}}_{\ell+1} - \vec{\mathbf{x}}_\ell|/|\vec{\mathbf{x}}_\ell| < 10^{-4}$. The fact that not a single partial differential equation has to be solved during the optimization process makes this algorithm particularly efficient.

6 Numerical results

In the numerical examples below we use $k = 1$ for the wave number, i.e., the wave length of the incident fields is $\lambda \approx 6.28$. To assess the numerical accuracy of the asymptotic representation formula (3.3), we have compared numerical approximations of electric far field patterns corresponding to thin tubular scattering objects D_ρ that have on the one hand been computed using the C++ boundary element library Bempp [33], and on the other hand using the leading order term in the asymptotic perturbation formula (3.3). This limited study in [12] suggests that the approximations obtained from the leading order term in (3.3) are accurate within a relative error of less than 5% when the radius ρ of the thin tube D_ρ is less than 1.5% of the wave length of the incident field, i.e., when $\rho \lesssim 0.1$ in our setting. This is also the range of radii, where we expect the results of the following examples to be applicable.

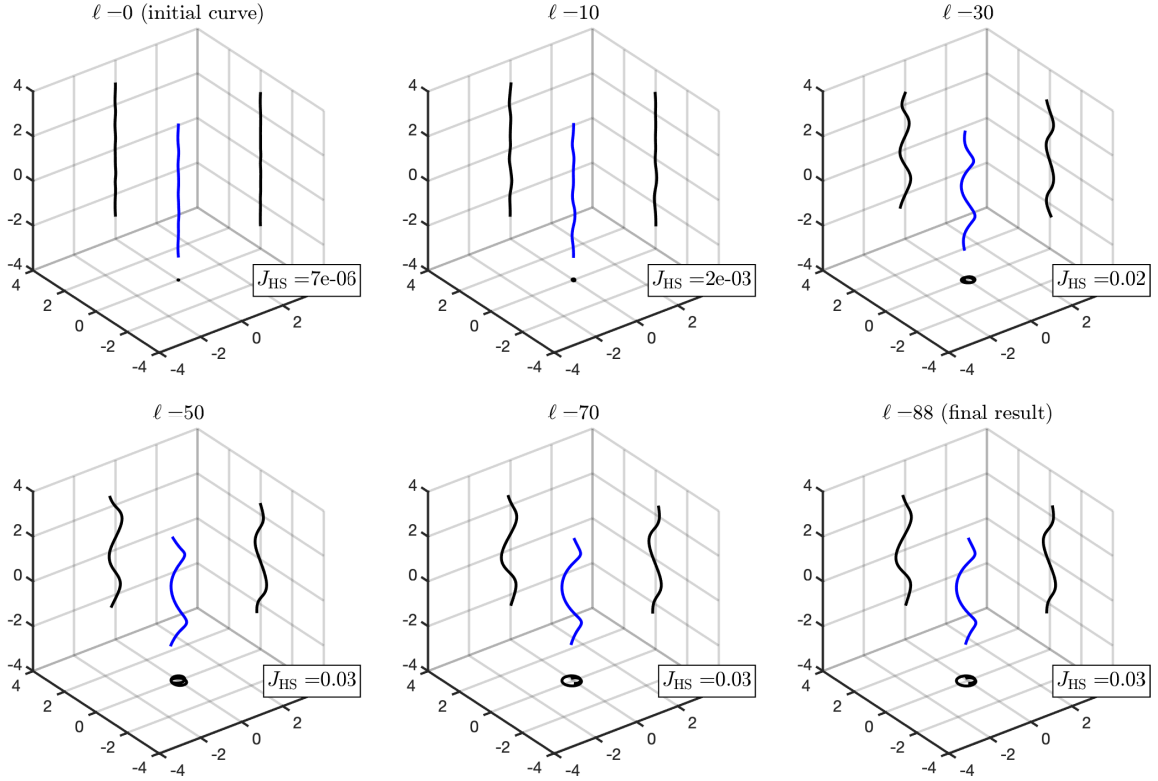


Figure 6.1: Convergence history for example 6.1. Top-left: Initial guess. Bottom-right: Final result.

Example 6.1. In the first example we consider the material parameters $\varepsilon_r = 5$ and $\mu_r = 1$. We use $\alpha_1 = 0.0005$ and $\alpha_2 = 0.5$ for the regularization parameters in (5.3), and the length constraint is chosen to be $L = 6$. For the initial guess \vec{x}_0 we consider $n = 20$ equidistant control points on the straight line segment between $(0, 0, -3)$ and $(0, 0, 3)$, and then we slightly perturb the first two components of each control point by adding random numbers between -0.02 and 0.02 . We note that the control points cannot be exactly on the straight line segment, because then the thin tubular scattering object with center curve $\mathbf{p}_\Delta[\vec{x}_0]$ would be em-achiral, and thus the objective functional Φ would not be differentiable at the initial guess.

Remark 3.3 recommends that the maximal degree N of vector spherical harmonics that is used in the basis representations of the operator $\mathbf{T}_\rho(\mathbf{p}_\Delta)$ (see lemma 3.2) and of its Fréchet derivative $\mathbf{T}'_\rho[\mathbf{p}_\Delta]\mathbf{h}$ (see remark 4.3) should be greater than R , where $B_R(0)$ is the smallest ball centered at the origin that contains the scattering object D_ρ . For this example we use $N = 5$.

In figure 6.1 we show the initial guess (top-left), some intermediate results that are obtained after $\ell = 10, 30, 50, 70$ iterations, and the final result (bottom-right) that is obtained after $\ell = 88$ iterations of the BFGS scheme. In each of these plots we also included the corresponding value of the relative chirality measure J_{HS} . During the optimization process the almost straight initial guess for the center curve winds up to a helix. The orientation of this helix in space and whether it is left or right turning depends on the orientation of the initial curve $\mathbf{p}_\Delta[\vec{x}_0]$, and on the particular values of the random perturbations that are used to set up the initial guess \vec{x}_0 .

In figure 6.2 (left) we show the evolution of the relative chirality measure J_{HS} during the optimization process. For comparison, we also include the corresponding values of the functional $J_2 : \mathcal{U}_{\text{ad}} \rightarrow [0, 1]$,

$$J_2(\mathbf{p}_\Gamma) := \frac{\chi_2(\mathbf{T}_\rho(\mathbf{p}_\Gamma))}{\|\mathbf{T}_\rho(\mathbf{p}_\Gamma)\|_{\text{HS}}},$$

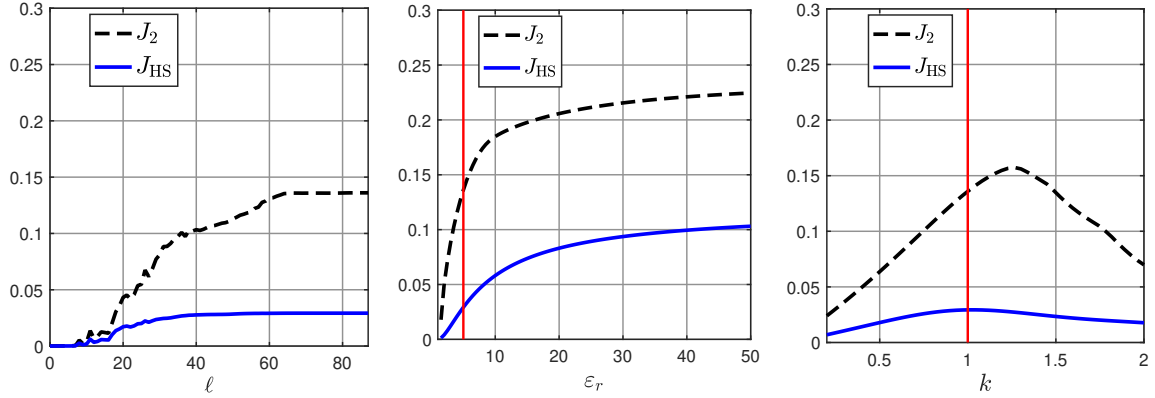


Figure 6.2: Normalized chirality measures J_{HS} and J_2 for example 6.1 with $L = 6$. Left: Evolution during BFGS iteration. Center: Sensitivity with respect to relative permittivity ε_r . Right: Sensitivity with respect to wavenumber k .

which is defined analogous to (5.1) but corresponds to the chirality measure χ_2 from (2.9) instead of χ_{HS} from (2.11). We observe that both functionals are increasing by several orders of magnitude during the optimization process, and that $J_{\text{HS}} \leq J_2$, in accordance with (2.12).

In figure 6.2 (center) we show plots of J_{HS} and J_2 for the optimized structure from figure 6.1 (bottom-right) as a function of ε_r , and in figure 6.2 (right) we show corresponding plots of J_{HS} and J_2 as a function of k . The vertical lines in these plots indicate the values of ε_r and k that have been used in the shape optimization (i.e., $\varepsilon_r = 5$ and $k = 1$). We observe that the relative chirality measures J_{HS} and J_2 are monotonically increasing in ε_r . On the other hand J_{HS} reaches a local maximum at the wave number $k = 1$ that has been used in the shape optimization, and there is a local maximum of J_2 close to this wave number. This suggests that the outcome of the optimization process is sensitive to the wave length of the incident field, and that the obtained optimality property is restricted to a rather narrow band of frequencies.

To study the dependence of the optimized center curve on the length constraint L in (5.2), we repeat the shape optimization with $L = 4$ and $L = 8$ instead of $L = 6$. The corresponding initial splines are shown in figure 6.3 (top-left and top-right). In accordance with remark 3.3 we choose $N = 4$ when $L = 4$, and $N = 6$ when $L = 8$ for the maximal degree N of vector spherical harmonics that is used in the basis representations of the operator $\mathbf{T}_\rho(\mathbf{p}_\Delta)$ and of its Fréchet derivative $\mathbf{T}'_\rho[\mathbf{p}_\Delta]\mathbf{h}$. In figure 6.3 (bottom-left and bottom-right) we show the final results that are obtained by the optimization procedure after 68 iterations (for $L = 4$) and after 92 iterations (for $L = 8$) of the BFGS scheme. For comparison we have also included the initial guess and the final result for $L = 6$ from figure 6.1 in the second column of figure 6.3. It is interesting to note that the diameters and the pitches of the three helices that are found by the optimization procedure are basically the same for the three different values of L , and that just the number of turns of the helix increases with increasing length constraint L . The relative chirality measures J_{HS} and J_2 attain essentially the same values for these three structures, but the total interaction cross-section increases with increasing values of L (not shown). \diamond

Example 6.2. In the second example we use $\varepsilon_r = 30$ and $\mu_r = 1$, i.e., the permittivity contrast is much larger than in the first example. We choose $\alpha_1 = 0.0001$ and $\alpha_2 = 0.1$ for the regularization parameters in (5.3), and the length constraint is $L = 20$.

For the initial guess \vec{x}_0 we consider $n = 45$ control points on a curve that given by two parallel line segments that are connected by a half circle as shown in figure 6.4 (top-left). The distance between the two vertical line segments is 2. Again we slightly perturb the first two components of each control point by adding random numbers between -0.02 and 0.02 to obtain

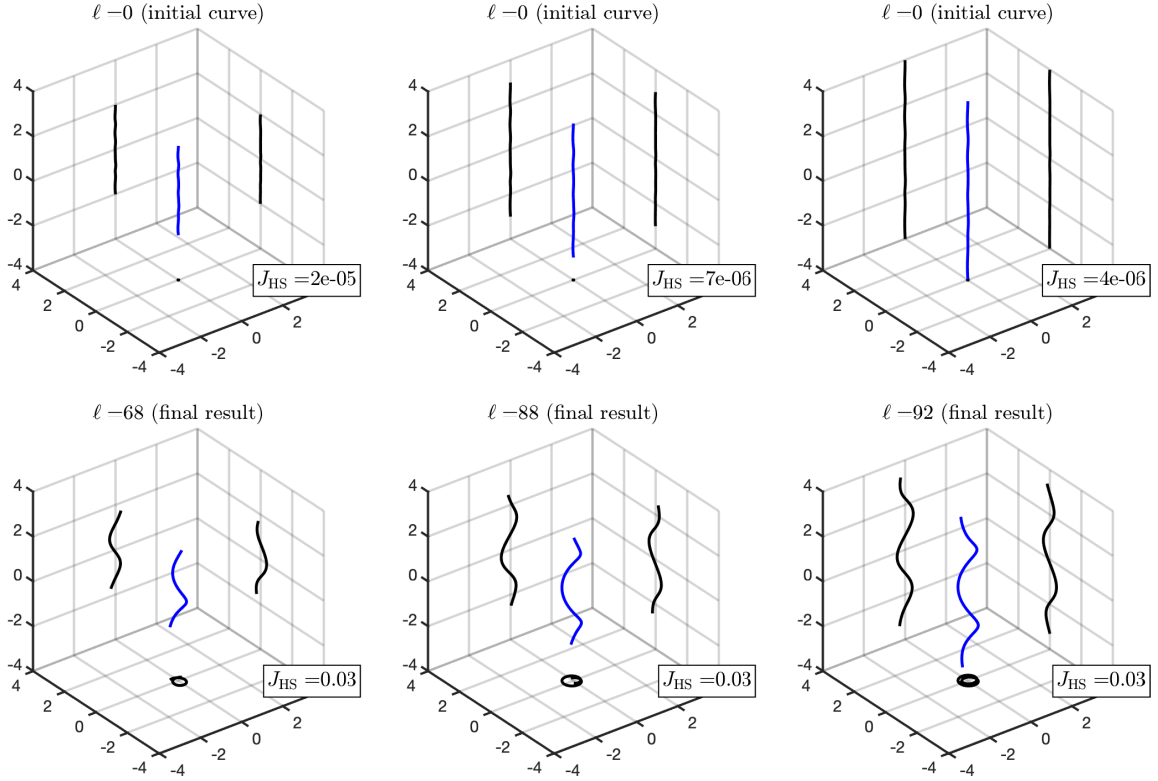


Figure 6.3: Optimal structures for different length constraints $L = 4, 6$ and 8 (left to right) in example 6.1. Top row: Initial guesses. Bottom row: Final results.

a well defined gradient of the objective functional at the initial guess. In accordance with remark 3.3 we use $N = 6$ for the maximal degree of vector spherical harmonics that is used in the basis representations of the operator $\mathbf{T}_\rho(\mathbf{p}_\Gamma)$ and of its Fréchet derivative $\mathbf{T}'_\rho[\mathbf{p}_\Gamma]\mathbf{h}$.

In figure 6.4 we show the initial guess (top-left), some intermediate results that are obtained after $\ell = 10, 30, 50, 70$ iterations, and the final result (bottom-right) that is obtained after $\ell = 189$ iterations of the BFGS scheme. During the optimization process the U-shaped initial guess winds up to a double helix.

In figure 6.5 (left) we show the evolution of the relative chirality measures J_{HS} and J_2 during the optimization process. As in Example 6.1 both functionals increase by several orders of magnitude during the optimization process. Figure 6.5 (center) shows plots of J_{HS} and J_2 for the optimized structure from figure 6.4 (bottom-right) as a function of ε_r , and in figure 6.5 (right) we show corresponding plots of J_{HS} and J_2 as a function of k . The vertical lines in these plots indicate the values of ε_r and k that have been used in the shape optimization (i.e., $\varepsilon_r = 30$ and $k = 1$). The relative chirality measures J_{HS} and J_2 are monotonically increasing in ε_r . On the other hand J_{HS} reaches a local maximum at $k = 1$, which is the wave number that has been used in the shape optimization, and there is a local maximum of J_2 close to this wave number. The sensitivity of both relative chirality measures with respect to the wave number is more pronounced than in example 6.1.

To study the dependence of the optimized center curve on the length constraint L , we repeat the shape optimization with $L = 15$ and $L = 25$ instead of $L = 20$. The corresponding initial splines are shown in figure 6.6 (top-left and top-right). In accordance with remark 3.3 we choose $N = 5$ when $L = 15$, and $N = 7$ when $L = 25$ for the maximal degree N of vector spherical harmonics that is used in the basis representations of the operator $\mathbf{T}_\rho(\mathbf{p}_\Delta)$ and of its Fréchet

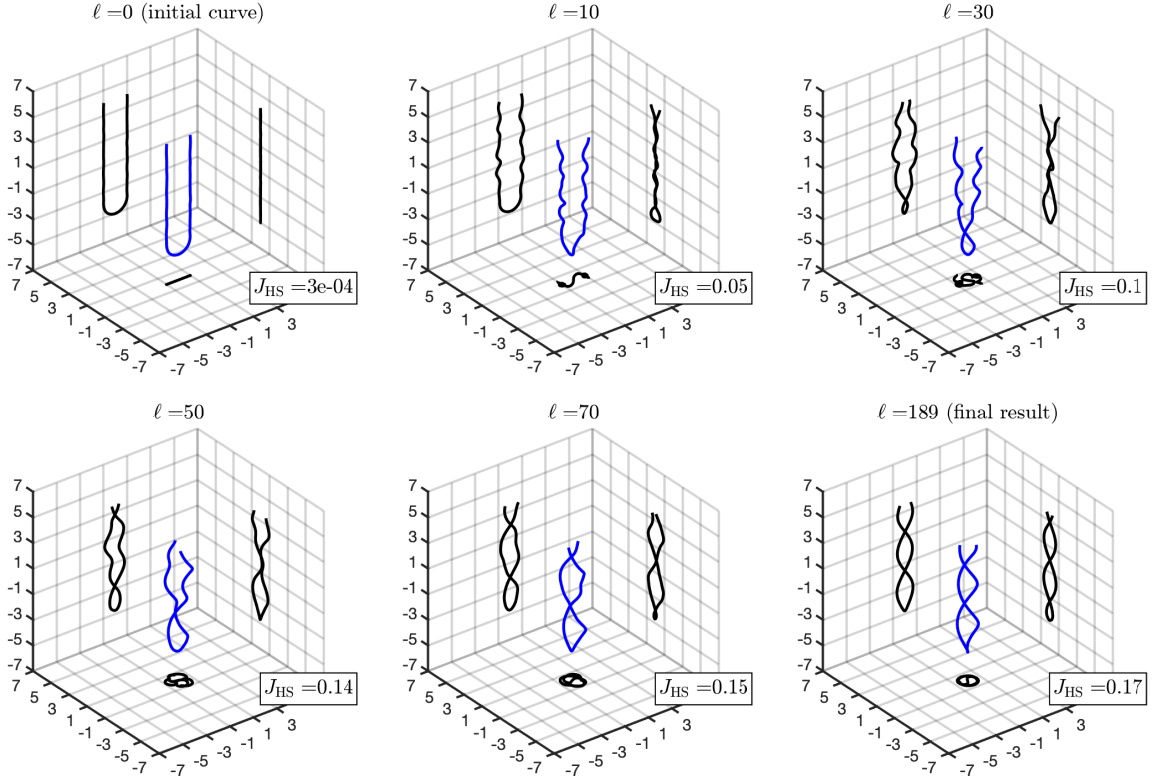


Figure 6.4: Convergence history for example 6.2. Top-left: Initial guess. Bottom-right: Final result.

derivative $T'_\rho[\mathbf{p}_\Delta]\mathbf{h}$. In figure 6.6 (bottom-left and bottom-right) we show the final results that are obtained by the optimization procedure after 109 iterations (for $L = 15$) and after 158 iterations (for $L = 25$) of the BFGS scheme. For comparison we have also included the initial guess and the final result for $L = 20$ from figure 6.4 in the second column of figure 6.6. As we already observed in Example 6.1 for the helix, the diameters and the pitches of the three double-helices that are found by the optimization procedure are basically the same for the three different values of L , and just the number of turns of the double-helix increases with increasing length constraint L . The relative chirality measures J_{HS} and J_2 attain essentially the same values for these three structures, but the total interaction cross section increases with increasing values of L . \diamond

Conclusions

Electromagnetic chirality measures quantify differences in the response of scattering objects or media due to left and right circularly polarized incident waves. We have considered the shape optimization problem to design dielectric thin tubular scattering objects with comparatively large measures of electromagnetic chirality.

We have applied an asymptotic representation formula for the scattered electromagnetic field due to such thin tubular structures to develop an efficient iterative shape optimization scheme. Our numerical results suggest that thin helical structures are candidates for optimal thin tubular scatterers, and that high electric permittivity contrasts increase the chiral effect. We also found that the chirality measure of optimized structures decays rather quickly if a different frequency than the frequency that is used for the shape optimization is considered.

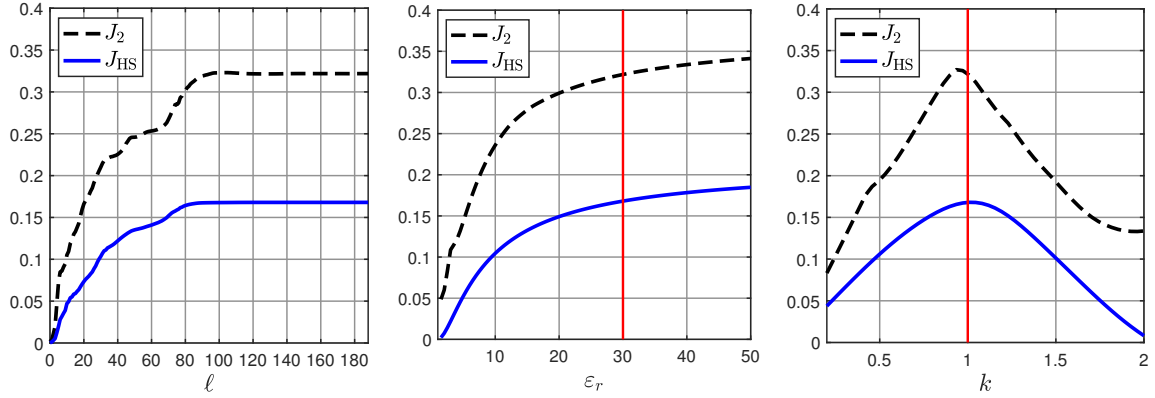


Figure 6.5: Normalized chirality measures J_{HS} and J_2 for example 6.2 with $L = 20$. Left: Evolution during BFGS iteration. Center: Sensitivity with respect to relative permittivity ε_r . Right: Sensitivity with respect to wavenumber k .

We have restricted the discussion to dielectric scattering objects because the asymptotic representation formula from [12] has so far only been justified in this case. An extension of the asymptotic representation formula to metallic scatterers and the shape optimization for metallic thin tubular structures will be the subject of future work.

Appendix

A Derivatives of spherical vector wave functions

The explicit basis representation of the Fréchet derivative $\mathbf{T}'_\rho[\mathbf{p}_\Gamma]\mathbf{h}$ in remark 4.3 contains derivatives of the circularly polarized spherical vector wave functions \mathbf{P}_n^m and \mathbf{Q}_n^m , $m = -n, \dots, n$, $n = 1, 2, \dots$. Recalling the definition of \mathbf{P}_n^m and \mathbf{Q}_n^m in (3.10), we provide a detailed discussion of the derivatives of the spherical vector wave functions \mathbf{M}_n^m from (3.9) and

$$\mathbf{curl} \mathbf{M}_n^m(\mathbf{x}) = \frac{\sqrt{n(n+1)}}{r} j_n(kr) Y_n^m(\hat{\mathbf{x}}) \hat{\mathbf{x}} + \frac{1}{r} (j_n(kr) + kr j_n'(kr)) \mathbf{U}_n^m(\hat{\mathbf{x}}), \quad \mathbf{x} \in \mathbb{R}^3,$$

(see, e.g., [26, thm. 2.43]). Both functions are best expressed in spherical coordinates,

$$\mathbf{x} = \begin{bmatrix} x_1 \\ x_2 \\ x_3 \end{bmatrix} = r \begin{bmatrix} \sin(\theta) \cos(\varphi) \\ \sin(\theta) \sin(\varphi) \\ \cos(\theta) \end{bmatrix} =: \boldsymbol{\psi}(r, \theta, \varphi), \quad r > 0, \theta \in [0, \pi], \varphi \in [0, 2\pi),$$

and consist of terms of the form $\mathbf{F}(\mathbf{x}) = J(r)\mathbf{W}(\theta, \varphi)$, where \mathbf{W} is one of the vector spherical harmonics $Y_n^m \hat{\mathbf{x}}$, \mathbf{U}_n^m , or \mathbf{V}_n^m . Using the chain rule

$$(\mathbf{F} \circ \boldsymbol{\psi})' = (\mathbf{F}' \circ \boldsymbol{\psi}) \boldsymbol{\psi}'$$

and observing that $(\boldsymbol{\psi}')^{-1}$ is known explicitly, it suffices to compute the partial derivatives of \mathbf{M}_n^m and $\mathbf{curl} \mathbf{M}_n^m$ with respect to the spherical coordinates. More precisely, with the spherical unit coordinate vectors

$$\hat{\mathbf{x}} := \begin{bmatrix} \sin(\theta) \cos(\varphi) \\ \sin(\theta) \sin(\varphi) \\ \cos(\theta) \end{bmatrix}, \quad \hat{\boldsymbol{\theta}} := \begin{bmatrix} \cos(\theta) \cos(\varphi) \\ \cos(\theta) \sin(\varphi) \\ -\sin(\theta) \end{bmatrix}, \quad \hat{\boldsymbol{\varphi}} := \begin{bmatrix} -\sin(\varphi) \\ \cos(\varphi) \\ 0 \end{bmatrix},$$

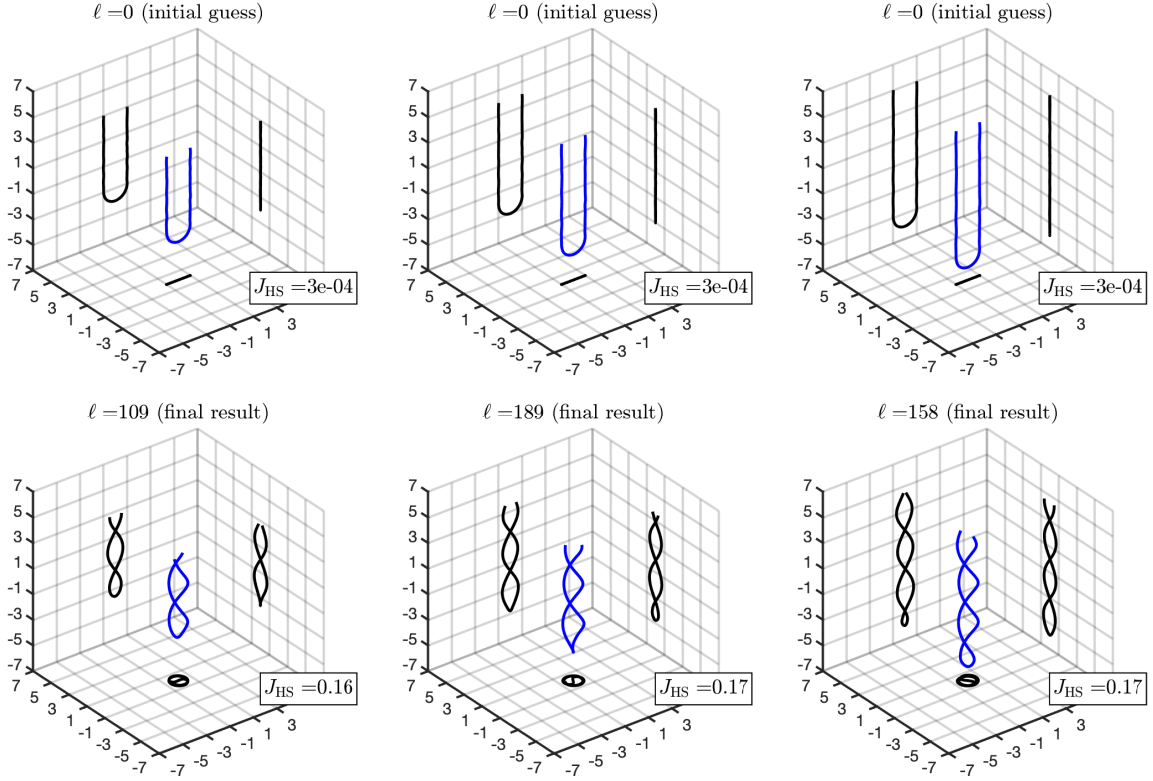


Figure 6.6: Optimal structures for different length constraints $L = 15, 20$ and 25 (left to right) in example 6.2. Top row: Initial guesses. Bottom row: Final results.

we obtain

$$\psi'(r, \theta, \varphi) = [\hat{\mathbf{x}} \mid \hat{\boldsymbol{\theta}} \mid \hat{\boldsymbol{\varphi}}] \begin{bmatrix} 1 & 0 & 0 \\ 0 & r & 0 \\ 0 & 0 & r \sin(\theta) \end{bmatrix},$$

and hence

$$\mathbf{F}' \circ \psi = \left[\frac{\partial J}{\partial r} \mathbf{W} \mid \frac{1}{r} J \frac{\partial \mathbf{W}}{\partial \theta} \mid \frac{1}{r \sin(\theta)} J \frac{\partial \mathbf{W}}{\partial \varphi} \right] \begin{bmatrix} \hat{\mathbf{x}}^\top \\ \hat{\boldsymbol{\theta}}^\top \\ \hat{\boldsymbol{\varphi}}^\top \end{bmatrix}. \quad (\text{A.1})$$

Note that throughout this section, we will surpress the dependence on r , θ and φ of the unit coordinate vectors and most other functions.

We start with the factors in \mathbf{M}_n^m and $\mathbf{curl} \mathbf{M}_n^m$ that depend only on the angular variables θ and φ and express their derivatives in terms of the spherical harmonics Y_n^m and the partial derivative of Y_n^m with respect to θ . First, we note that the derivatives of the unit coordinate vectors satisfy

$$\begin{aligned} \partial_\theta \hat{\mathbf{x}} &= \hat{\boldsymbol{\theta}}, & \partial_\theta \hat{\boldsymbol{\theta}} &= -\hat{\mathbf{x}}, & \partial_\theta \hat{\boldsymbol{\varphi}} &= 0, \\ \partial_\varphi \hat{\mathbf{x}} &= \sin(\theta) \hat{\boldsymbol{\varphi}}, & \partial_\varphi \hat{\boldsymbol{\theta}} &= \cos(\theta) \hat{\boldsymbol{\varphi}}, & \partial_\varphi \hat{\boldsymbol{\varphi}} &= -\sin(\theta) \hat{\mathbf{x}} - \cos(\theta) \hat{\boldsymbol{\theta}}. \end{aligned}$$

A particular choice of spherical harmonics Y_n^m , $m = -n, \dots, n$, $n = 0, 1, \dots$, is obtained from the definition

$$Y_n^m := C_n^m P_n^{|m|}(\cos(\theta)) e^{im\varphi} \quad \text{with} \quad C_n^m := \sqrt{\frac{2n+1}{4\pi} \frac{(n-|m|)!}{(n+|m|)!}}, \quad (\text{A.2})$$

where $P_n^m(t) := (1-t^2)^{m/2}(\mathrm{d}/\mathrm{d}t)^m P_n(t)$, $m = 0, \dots, n$, denote the associated Legendre functions (see, e.g., [26, p. 41]). Derivatives of Y_n^m with respect to φ just amount to multiplications with powers of im . The first derivative of Y_n^m with respect to θ is calculated explicitly from

$$\begin{aligned} \frac{\mathrm{d}P_n^m}{\mathrm{d}t}(t) &= -mt(1-t^2)^{(m-2)/2} \frac{\mathrm{d}^m P_n}{\mathrm{d}t^m}(t) + (1-t^2)^{m/2} \frac{\mathrm{d}^{m+1} P_n}{\mathrm{d}t^{m+1}}(t) \\ &= \frac{1}{(1-t^2)^{1/2}} P_n^{m+1}(t) - \frac{mt}{1-t^2} P_n^m(t), \quad n \in \mathbb{N}, m = 0, \dots, n, \end{aligned}$$

which gives

$$\partial_\theta Y_n^m = m \cot(\theta) Y_n^m - \frac{C_n^m}{C_n^{m+1}} e^{-i\varphi} Y_n^{m+1} \quad \text{and} \quad \partial_\theta Y_n^{-m} = \overline{\partial_\theta Y_n^m} \quad (\text{A.3})$$

for $n \in \mathbb{N}$ and $m = 0, \dots, n$. Here, we use $P_n^{n+1} := 0$ and $Y_n^{n+1} := 0$ for convenience of notation.

As spherical harmonics are eigenfunctions of the Laplace-Beltrami operator on the unit sphere,

$$\frac{1}{\sin \theta} \partial_\theta (\sin(\theta) \partial_\theta Y_n^m) + \frac{1}{\sin^2(\theta)} \partial_\varphi^2 Y_n^m = -n(n+1) Y_n^m, \quad (\text{A.4})$$

(see, e.g., [26, p. 41]) we can compute the second derivative of Y_n^m with respect to θ as

$$\partial_\theta^2 Y_n^m = -\cot(\theta) \partial_\theta Y_n^m + \left(\frac{m^2}{\sin^2(\theta)} - n(n+1) \right) Y_n^m. \quad (\text{A.5})$$

We apply these formulas to find expressions for the derivatives of the vector spherical harmonics $Y_n^m \hat{\mathbf{x}}$, \mathbf{U}_n^m , and \mathbf{V}_n^m with respect to θ and φ . For the radially oriented $Y_n^m \hat{\mathbf{x}}$ we obtain

$$\partial_\theta (Y_n^m \hat{\mathbf{x}}) = \partial_\theta Y_n^m \hat{\mathbf{x}} + Y_n^m \hat{\boldsymbol{\theta}}, \quad (\text{A.6a})$$

$$\frac{1}{\sin(\theta)} \partial_\varphi (Y_n^m \hat{\mathbf{x}}) = \frac{im}{\sin(\theta)} Y_n^m \hat{\mathbf{x}} + Y_n^m \hat{\boldsymbol{\varphi}}. \quad (\text{A.6b})$$

From the definition (3.6) we find for \mathbf{U}_n^m and \mathbf{V}_n^m that

$$\mathbf{U}_n^m = \frac{1}{\sqrt{n(n+1)}} \left(\partial_\theta Y_n^m \hat{\boldsymbol{\theta}} + \frac{im}{\sin(\theta)} Y_n^m \hat{\boldsymbol{\varphi}} \right), \quad (\text{A.7a})$$

$$\mathbf{V}_n^m = \frac{1}{\sqrt{n(n+1)}} \left(\partial_\theta Y_n^m \hat{\boldsymbol{\varphi}} - \frac{im}{\sin(\theta)} Y_n^m \hat{\boldsymbol{\theta}} \right). \quad (\text{A.7b})$$

We further deduce

$$\partial_\theta \mathbf{U}_n^m = \frac{1}{\sqrt{n(n+1)}} \left(-\partial_\theta Y_n^m \hat{\mathbf{x}} + \partial_\theta^2 Y_n^m \hat{\boldsymbol{\theta}} - \frac{im}{\sin(\theta)} (\cot(\theta) Y_n^m - \partial_\theta Y_n^m) \hat{\boldsymbol{\varphi}} \right), \quad (\text{A.8a})$$

$$\frac{1}{\sin(\theta)} \partial_\varphi \mathbf{U}_n^m = \frac{1}{\sqrt{n(n+1)}} \left(-\frac{im}{\sin(\theta)} Y_n^m \hat{\mathbf{x}} + \frac{im}{\sin(\theta)} (\partial_\theta Y_n^m - \cot(\theta) Y_n^m) \hat{\boldsymbol{\theta}} \right. \quad (\text{A.8b})$$

$$\left. + \left(\cot(\theta) \partial_\theta Y_n^m - \frac{m^2}{\sin^2(\theta)} Y_n^m \right) \hat{\boldsymbol{\varphi}} \right), \quad (\text{A.8c})$$

$$\partial_\theta \mathbf{V}_n^m = \frac{1}{\sqrt{n(n+1)}} \left(\frac{im}{\sin(\theta)} Y_n^m \hat{\mathbf{x}} + \frac{im}{\sin(\theta)} (\cot(\theta) Y_n^m - \partial_\theta Y_n^m) \hat{\boldsymbol{\theta}} + \partial_\theta^2 Y_n^m \hat{\boldsymbol{\varphi}} \right), \quad (\text{A.8d})$$

$$\frac{1}{\sin(\theta)} \partial_\varphi \mathbf{V}_n^m = \frac{1}{\sqrt{n(n+1)}} \left(-\partial_\theta Y_n^m \hat{\mathbf{x}} + \left(\frac{m^2}{\sin^2(\theta)} Y_n^m - \cot(\theta) \partial_\theta Y_n^m \right) \hat{\boldsymbol{\theta}} \right. \quad (\text{A.8e})$$

$$\left. + \frac{im}{\sin(\theta)} (\partial_\theta Y_n^m - \cot(\theta) Y_n^m) \hat{\boldsymbol{\varphi}} \right). \quad (\text{A.8f})$$

The representations (A.3)–(A.8) contain several terms that are ill-suited to numerical evaluation for θ close to 0 or π . These are

$$\frac{1}{\sin(\theta)}Y_n^m, \quad \frac{1}{\sin(\theta)}(\cot(\theta)Y_n^m - \partial_\theta Y_n^m), \quad \frac{m^2}{\sin^2(\theta)}Y_n^m - \cot(\theta)\partial_\theta Y_n^m. \quad (\text{A.9})$$

Note that the first two expressions in (A.9) always appear in combination with a factor m in (A.3)–(A.8) and thus are only relevant for $m \neq 0$. We will only consider $m \geq 0$ in the following paragraphs, as the corresponding formulas for negative m can immediately be obtained by complex conjugation.

To rewrite the first term in (A.9), we use the recurrence relation

$$\frac{P_n^m(t)}{\sqrt{1-t^2}} = \frac{1}{2mt} (P_n^{m+1}(t) + (n+m)(n-m+1)P_n^{m-1}(t)), \quad n \geq 2, m = 1, \dots, n-1,$$

for the associated Legendre functions (see, e.g., [26, p. 35]). Inserting this into (A.2) gives

$$\frac{Y_n^m}{\sin(\theta)} = \frac{C_n^m}{2m \cos(\theta)} \left(\frac{e^{-i\varphi}}{C_n^{m+1}} Y_n^{m+1} + \frac{(n+m)(n-m+1)e^{i\varphi}}{C_n^{m-1}} Y_n^{m-1} \right) \quad (\text{A.10})$$

for $n \geq 2$ and $m = 1, \dots, n-1$. Furthermore, differentiating Rodrigues' formula for the associated Legendre functions (see, e.g., [26, thm. 2.6]) n times shows that $P_n^n(\cos(\theta)) = \frac{(2n)!}{2^n n!} \sin^n(\theta)$. Therefore,

$$\frac{Y_n^n}{\sin(\theta)} = C_n^n \frac{(2n)!}{2^n n!} \sin^{n-1}(\theta) e^{in\varphi}, \quad n \in \mathbb{N}. \quad (\text{A.11})$$

For the second term in (A.9), from (A.3) we have that

$$\frac{1}{\sin(\theta)}(\cot(\theta)Y_n^m - \partial_\theta Y_n^m) = \frac{C_n^m}{C_n^{m+1}} e^{-i\varphi} \frac{Y_n^{m+1}}{\sin(\theta)} - (m-1) \cos(\theta) \frac{Y_n^m}{\sin^2(\theta)}. \quad (\text{A.12})$$

For $m = 1$, this can be evaluated using (A.10). For $n \geq 2$ and $m = 2, \dots, n$, expressions for $\sin^{-2}(\theta)Y_n^m$ are immediately obtained from (A.10) and (A.11).

Finally, the third term in (A.9) satisfies

$$\frac{m^2}{\sin^2(\theta)}Y_n^m - \cot(\theta)\partial_\theta Y_n^m = \frac{C_n^m}{C_n^{m+1}} e^{-i\varphi} \cos(\theta) \frac{Y_n^{m+1}}{\sin(\theta)} + (m^2 - m \cos^2(\theta)) \frac{Y_n^m}{\sin^2(\theta)}. \quad (\text{A.13})$$

For $n, m \geq 2$, no new issues arise, and for $m = 1$, the last term on the right hand side of (A.13) reduces to Y_n^1 . In (A.13) we also have to consider the case $m = 0$, where (A.2) gives

$$-\cot(\theta)\partial_\theta Y_n^0 = -C_n^0 \cot(\theta)\partial_\theta P_n(\cos(\theta)) = C_n^0 \cos(\theta)P_n'(\cos(\theta)). \quad (\text{A.14})$$

For numerical implementations of (A.3), (A.5)–(A.8) we suggest to use the expressions directly when $\theta \in [\pi/4, 3\pi/4]$, and to replace the problematic terms with the expressions from (A.10)–(A.14) when $\theta \in [0, \pi/4]$ or $\theta \in (3\pi/4, \pi]$.

We continue with the factors in \mathbf{M}_n^m and $\mathbf{curl} \mathbf{M}_n^m$ that depend only on the radial variable r , i.e.,

$$j_n(kr), \quad \frac{j_n(kr)}{r}, \quad \frac{j_n(kr) + kr j_n'(kr)}{r}. \quad (\text{A.15})$$

We require the derivatives

$$\begin{aligned} \partial_r j_n(kr) &= k j_n'(kr), \\ \partial_r \frac{j_n(kr)}{r} &= \frac{kr j_n'(kr) - j_n(kr)}{r^2}, \\ \partial_r \left(\frac{j_n(kr) + kr j_n'(kr)}{r} \right) &= \frac{(kr)^2 j_n''(kr) + kr j_n'(kr) - j_n(kr)}{r^2}. \end{aligned}$$

These may be simplified using the spherical Bessel differential equation

$$t^2 j_n''(t) + 2t j_n'(t) + (t^2 - n(n+1))j_n(t) = 0$$

(see, e.g., [26, p. 54]) and the recurrence relation

$$j_n'(t) = \frac{n}{t} j_n(t) - j_{n+1}(t)$$

(see, e.g., [28, 10.51.2]) to obtain

$$\partial_r j_n(kr) = \frac{n}{r} j_n(kr) - k j_{n+1}(kr), \quad (\text{A.16a})$$

$$\partial_r \frac{j_n(kr)}{r} = \frac{(n-1)j_n(kr) - kr j_{n+1}(kr)}{r^2}, \quad (\text{A.16b})$$

$$\begin{aligned} \partial_r \frac{j_n(kr) + kr j_n'(kr)}{r} &= \frac{-kr j_n'(kr) + (n(n+1) - 1 - (kr)^2)j_n(kr)}{r^2} \\ &= \frac{kr j_{n+1}(kr) + (n^2 - 1 - (kr)^2)j_n(kr)}{r^2}. \end{aligned} \quad (\text{A.16c})$$

For small values of $r > 0$, the expansion of the spherical Bessel functions in powers of r (see, e.g., [26, dfn. 2.26]) should be inserted into (A.15) and (A.16) and being truncated to a finite sum for numerical evaluation. In particular, we note that for $n = 1$ negative powers of r seem to remain in (A.1) when the two summands in $\mathbf{curl} \mathbf{M}_n^m$ are inserted separately. However, some tedious calculations show that these terms cancel as expected when the sum is formed. Hence, for numerical evaluation in the case $n = 1$, all terms of order r^{-1} should be left out of the calculation to avoid cancellation effects.

Acknowledgments

Funded by the Deutsche Forschungsgemeinschaft (DFG, German Research Foundation) – Project-ID 258734477 – SFB 1173. The authors would like to thank I. Fernandez-Corbaton, X. Garcia-Santiago, and C. Rockstuhl for many interesting discussions related to the subject of this paper.

References

- [1] G. S. Alberti and Y. Capdeboscq. *Lectures on elliptic methods for hybrid inverse problems*, volume 25 of *Cours Spécialisés*. Société Mathématique de France, Paris, 2018.
- [2] H. Ammari, K. Hamdache, and J.-C. Nédélec. Chirality in the Maxwell equations by the dipole approximation. *SIAM J. Appl. Math.*, 59(6):2045–2059, 1999.
- [3] H. Ammari, M. S. Vogelius, and D. Volkov. Asymptotic formulas for perturbations in the electromagnetic fields due to the presence of inhomogeneities of small diameter. II. The full Maxwell equations. *J. Math. Pures Appl. (9)*, 80(8):769–814, 2001.
- [4] H. Ammari and D. Volkov. The leading-order term in the asymptotic expansion of the scattering amplitude of a collection of finite number of dielectric inhomogeneities of small diameter. *International Journal for Multiscale Computational Engineering*, 3(3), 2005.
- [5] T. Arens, F. Hagemann, F. Hettlich, and A. Kirsch. The definition and measurement of electromagnetic chirality. *Math. Methods Appl. Sci.*, 41(2):559–572, 2018.
- [6] C. Athanasiadis, P. A. Martin, and I. G. Stratis. Electromagnetic scattering by a homogeneous chiral obstacle: boundary integral equations and low-chirality approximations. *SIAM J. Appl. Math.*, 59(5):1745–1762, 1999.

- [7] C. Athanasiadis, P. A. Martin, and I. G. Stratis. Electromagnetic scattering by a homogeneous chiral obstacle: scattering relations and the far-field operator. *Math. Methods Appl. Sci.*, 22(14):1175–1188, 1999.
- [8] E. Beretta, Y. Capdeboscq, F. de Gournay, and E. Francini. Thin cylindrical conductivity inclusions in a three-dimensional domain: a polarization tensor and unique determination from boundary data. *Inverse Problems*, 25(6):065004, 22, 2009.
- [9] Y. Capdeboscq and M. S. Vogelius. A general representation formula for boundary voltage perturbations caused by internal conductivity inhomogeneities of low volume fraction. *M2AN Math. Model. Numer. Anal.*, 37(1):159–173, 2003.
- [10] Y. Capdeboscq and M. S. Vogelius. Optimal asymptotic estimates for the volume of internal inhomogeneities in terms of multiple boundary measurements. *M2AN Math. Model. Numer. Anal.*, 37(2):227–240, 2003.
- [11] Y. Capdeboscq and M. S. Vogelius. Pointwise polarization tensor bounds, and applications to voltage perturbations caused by thin inhomogeneities. *Asymptot. Anal.*, 50(3-4):175–204, 2006.
- [12] Y. Capdeboscq, R. Griesmaier, and M. Knöller. An asymptotic representation formula for scattering by thin tubular structures and an application in inverse scattering. *Submitted*, 2020.
- [13] D. Colton and R. Kress. *Inverse acoustic and electromagnetic scattering theory*, volume 93 of *Applied Mathematical Sciences*. Springer, Cham, 2019. 4th ed.
- [14] M. Decker, M. Klein, M. Wegener, and S. Linden. Circular dichroism of planar chiral magnetic metamaterials. *Optics letters*, 32(7):856–858, 2007.
- [15] N. Dunford and J. T. Schwartz. *Linear operators. Part II: Spectral theory. Self adjoint operators in Hilbert space*. With the assistance of William G. Bade and Robert G. Bartle. Interscience Publishers John Wiley & Sons New York-London, 1963.
- [16] I. Fernandez-Corbaton, M. Fruhnert, and C. Rockstuhl. Objects of maximum electromagnetic chirality. *Physical Review X*, 6(3):031013, 2016.
- [17] J. K. Gansel, M. Thiel, M. S. Rill, M. Decker, K. Bade, V. Saile, G. von Freymann, S. Linden, and M. Wegener. Gold helix photonic metamaterial as broadband circular polarizer. *Science*, 325(5947):1513–1515, 2009.
- [18] R. Griesmaier. Reconstruction of thin tubular inclusions in three-dimensional domains using electrical impedance tomography. *SIAM J. Imaging Sci.*, 3(3):340–362, 2010.
- [19] R. Griesmaier. A general perturbation formula for electromagnetic fields in presence of low volume scatterers. *ESAIM Math. Model. Numer. Anal.*, 45(6):1193–1218, 2011.
- [20] R. Griesmaier and N. Hyvönen. A regularized Newton method for locating thin tubular conductivity inhomogeneities. *Inverse Problems*, 27(11):115008, 22, 2011.
- [21] R. Griesmaier and J. Sylvester. Uncertainty principles for inverse source problems for electromagnetic and elastic waves. *Inverse Problems*, 34(6):065003, 37, 2018.
- [22] F. Hagemann. *Reconstructing the shape and measuring chirality of obstacles in electromagnetic scattering*. PhD thesis, Karlsruhe Institute of Technology (KIT), 2019.
- [23] F. Hagemann, T. Arens, T. Betcke, and F. Hettlich. Solving inverse electromagnetic scattering problems via domain derivatives. *Inverse Problems*, 35(8):084005, 20, 2019.
- [24] F. Hettlich. The domain derivative of time-harmonic electromagnetic waves at interfaces. *Math. Methods Appl. Sci.*, 35(14):1681–1689, 2012.
- [25] R. Hiptmair and J. Li. Shape derivatives for scattering problems. *Inverse Problems*, 34(10):105001, 25, 2018.
- [26] A. Kirsch and F. Hettlich. *The mathematical theory of time-harmonic Maxwell’s equations*, volume 190 of *Applied Mathematical Sciences*. Springer, Cham, 2015. Expansion-, integral-, and variational methods.

- [27] D.-H. Li and M. Fukushima. On the global convergence of the BFGS method for nonconvex unconstrained optimization problems. *SIAM J. Optim.*, 11(4):1054–1064, 2001.
- [28] F. W. J. Olver, D. W. Lozier, R. F. Boisvert, and C. W. Clark, editors. *NIST handbook of mathematical functions*. U.S. Department of Commerce, National Institute of Standards and Technology, Washington, DC; Cambridge University Press, Cambridge, 2010.
- [29] J. Pendry. A chiral route to negative refraction. *Science*, 306(5700):1353–1355, 2004.
- [30] E. Plum, J. Zhou, J. Dong, V. Fedotov, T. Koschny, C. Soukoulis, and N. Zheludev. Metamaterial with negative index due to chirality. *Physical Review B*, 79(3):035407, 2009.
- [31] R. Potthast. Domain derivatives in electromagnetic scattering. *Math. Methods Appl. Sci.*, 19(15):1157–1175, 1996.
- [32] A. Rogacheva, V. Fedotov, A. Schwanecke, and N. Zheludev. Giant gyrotropy due to electromagnetic-field coupling in a bilayered chiral structure. *Physical review letters*, 97(17):177401, 2006.
- [33] W. Śmigaj, T. Betcke, S. Arridge, J. Phillips, and M. Schweiger. Solving boundary integral problems with BEM++. *ACM Trans. Math. Software*, 41(2):Art. 6, 40, 2015.
- [34] S. Zhang, Y.-S. Park, J. Li, X. Lu, W. Zhang, and X. Zhang. Negative refractive index in chiral metamaterials. *Physical review letters*, 102(2):023901, 2009.